Development of Design Guidelines for CIP Joint Connections with U-bar Reinforcement

A Thesis

Presented for the

Master of Science Degree

The University of Tennessee, Knoxville

Richard Aaron Hanks

May 2011

Acknowledgements

I would like to thank my wife, Julie Hanks, parents, Richard and Glenda Hanks, and the rest of my family for their support and encouragement in pursuing a career in Structural Engineering. My education and career would not have been possible without their love and support. I would especially like to thank Dr. John Ma for encouraging and guiding me in pursuit of a Master of Science degree by providing this excellent opportunity to further my education to an important and applicable research project. Thanks to Beth Chapman and Sam Lewis for their exhaustive lab results and information. I am grateful for Zhiqi He for providing assistance in the strut and tie modeling. Thanks to Qi Cao for presenting and helping to navigate through the lab results. I would also like to thank Dr. Edwin Burdette for providing his professional expertise in reinforced concrete. My extended thanks go to Dr. Burdette and Dr. Qiuhong Zhao for being on my committee.

Abstract

The interstate highway system is vitally dependent upon current and future bridges. These bridges must be designed economically to continue the serviceability with limited maintenance. For precast bridge construction a portion of the design must consider the bridge connections. Some current connections have proved insufficient in serviceability as there is uncontrolled cracking. In other connections there are uncertainties in the calculations (or lack of calculations) which require design guidelines.

This thesis presents design recommendations for precast decking u-bar reinforcement in tension which results from negative moment over a pier. Testing results from the University of Tennessee were analyzed to determine the design recommendations. The calculated capacity of the specimens was determined first by strut and tie modeling by AASHTO and ACI, but was shown to be insufficient.

Proposed changes to the current calculation of the strut width as specified in AASHTO and ACI STM methods were discussed in order to match the test results. However, strut and tie modeling demonstrated that the design for the lacer bar was inadequate. Since the strut and tie modeling method resulted in an inaccurate lacer bar size, another method was developed.

A triangular shape develops from the flow of forces in the connection joint zone; as a result, a free body diagram (FBD) was developed from the concrete triangular shape. This diagram showed how the forces flow in the in-situ joint as well as how they are resisted. A formula was developed from the FBD to determine the capacity of the joint which accurately reflected the capacities from tests.

A FBD was also made of the lacer bar utilizing the forces and geometry calculated from the capacity calculations. A computer analysis program was used to determine the forces in the lacer bar. The lacer bar could then be designed since the required forces to resist (moment and shear) were known.

A comparison of the strut and tie model to the triangular method led to the conclusion that both can determine the longitudinal reinforcement spacing, joint overlap length, and concrete strength, but only the triangular method can determine a more sufficient lacer bar size.

Table of Contents

Development of Design Guidelines for CIP Joint Connections with U-bar Reinforcement i

Chapter 1 Introduction 1

1.1 Introduction 1

1.2 Lab Research 2

1.3 Literature Review 7

Chapter 2 Strut and Tie Modeling 11

2.1 STM for the joint connections 11

2.2 ACI strut and tie modeling 11

2.3 AASHTO strut and tie modeling 14

2.4 Adjusted joint strut and tie model 14

Chapter 3 Triangular Method 20

3.1 Tension Joint Capacity Calculations 20

3.2 Lacer Bar 27

Chapter 4 Recommended Design Criteria for the Triangular Method 41

4.1 Area Calculations of the Bearing Strength Capacity 41

4.2 Limitations of design 43

4.2.1 Concrete compressive strength 44

4.2.2 U-bar spacing 44

4.2.3 Overlap length 46

4.3 Lacer Bar 48

Chapter 5 Conclusion 55

List of References 58

Vita 61

List of Tables

Table 1: Testing parameters and capacities of tensile specimens 7
Table 2: Maximum forces in their respective joints..... 12
Table 3: STM calculated capacity verses testing 17
Table 4: Calculated verses tested capacities dependent upon different variables..... 26
Table 5: Area design calculations comparison..... 43
Table 6: U-bar spacing capacity comparison of per triangle and per foot section..... 45
Table 7: Joint overlap length capacity comparison..... 47
Table 8: Comparison of elastic and plastic design..... 51
Table 9: Deflection comparison of ST-0 for different rebar sizes..... 53

List of Figures

Figure 1: A current precast concrete decking joint connection 1
Figure 2: U-bar transverse joint 3
Figure 3: Headed bar transverse joint 4
Figure 4: U-bar joint detail strain gauge configuration 4
Figure 5: Headed Bar joint detail strain gauge configuration 5
Figure 6: Tensile specimens WT-1, WT-2, WT-3, ST-0, ST-7, FT-0, and FT-7 with varying parameters shown in Table 1 6
Figure 7: Tensile specimen WT-4 with parameters shown in Table 1 7
Figure 8: STM of joint section 12
Figure 9: Width of the strut 15
Figure 10: STM tested capacities verses calculated capacities based on f'_c 17
Figure 11: Concrete triangular formation 20
Figure 12: Triangular method 22
Figure 13: U-bar transverse joint specimen 24
Figure 14: Triangular Method calculated verses tested capacities based on f'_c 26
Figure 15: WT-2 Top of the Lacer Bar 28
Figure 16: WT-4 Lacer Bar 28
Figure 17: (ω_{CONC}) Concrete bearing reaction to the lacer bar deflection 31
Figure 18: Loading configuration of the lacer bar where loading controls 32
Figure 19: Loading configuration of the lacer bar where bearing controls 32
Figure 20: ω_L locations 33
Figure 21: ω_B locations 33
Figure 22: ω_{CONC} locations 33
Figure 23: Deflected shape of the lacer bar according to the proposed model 35
Figure 24: ST-0 lacer bar from loading side 37
Figure 25: Deflected shape of lacer bar of specimen ST-0 according to rules given 37
Figure 26: Deflected shape of lacer bar of specimen ST-0 according to the adjusted model 37
Figure 27: ST-0 lacer bar from loaded side compared to the adjusted model 38
Figure 28: ST-0 lacer bar from bearing side 39
Figure 29: ST-0 lacer bar from bearing modeled as defined 39
Figure 30: ST-0 lacer bar from bearing adjusted model 39
Figure 31: ST-0 lacer bar compared to the adjusted model deflection 40
Figure 32: Comparing area design calculations 43
Figure 33: U-bar spacing capacity comparison 45
Figure 34: Comparison of the number of triangles for u-bar spacing 45
Figure 35: Joint overlap length capacity comparison 47
Figure 36: Clear spacing between a #4 lacer bar and u-bar 52
Figure 37: Clear spacing for a #8 lacer bar 52
Figure 38: Deflection of ST-0 verses size of bar 54
Figure 39: Comparison of the triangular method and STM calculated capacities 56

Chapter 1 Introduction

1.1 Introduction

Precast concrete decks provide an economical solution for rapid bridge construction. Precast concrete decks must be connected on site so that the entire bridge functions as a unit to resist all applied loads. The deck must resist moment and shear induced from the loads as well as tensile forces which would take place over a pier. Negative moment is introduced at the pier location causing the deck to be in tension to resist the applied moment. An example of current decking joint connections is shown in Figure 1. As can be seen, this type of connection limits the bending resistance since the forces at the connection must be transferred by concrete. Thus, flexural cracks cannot be controlled which produces joint leakage.

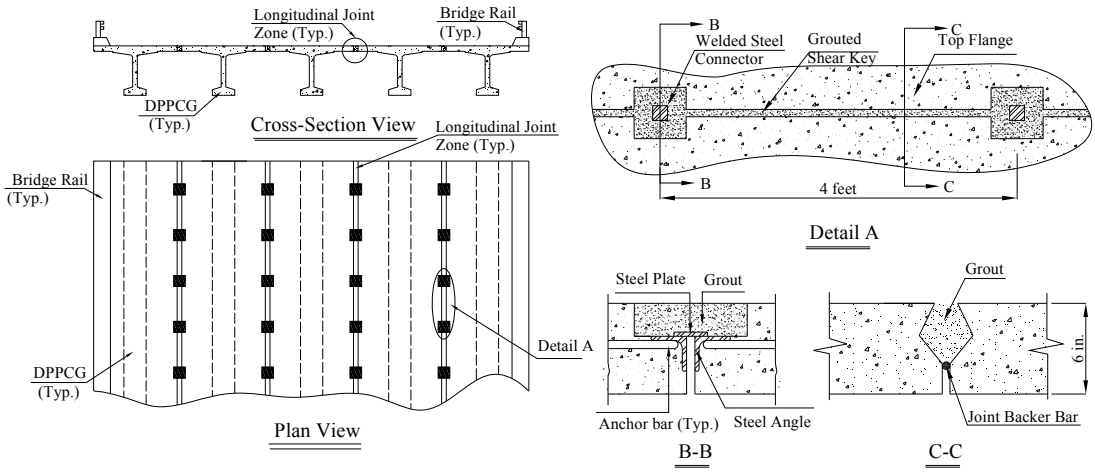

Figure 1: A current precast concrete decking joint connection

In order to provide a more functional connection, the University of Tennessee has provided extensive lab testing for different types of connections taking constructability, strength, and ductility into consideration (Lewis 2009 and Chapman

2010). U-bar connections proved to be the most beneficial for strength and ductility (Lewis 2009), but design recommendations have not been introduced.

This thesis provides a proposal for the design of u-bar reinforcement connections for the precast concrete deck undergoing tension. The method introduced will show how to determine the connection's capacity by considering the overlap joint length, u-bar spacing, concrete strength, and size of the lacer bar. In order to ensure that the u-bar reinforcement fails first (to provide ductility), the capacity and influence of the lacer bar must also be understood since the lacer bar improves the performance of the connection.

1.2 Lab Research

Testing of the in-situ joint connection has been done at the University of Tennessee by Sam Lewis (2009) and Beth Chapman (2010). There were two joint directions of the joints: a longitudinal joint and a transverse joint. The two different joints experienced different forces and had to be tested accordingly. The longitudinal joint was tested in bending since the decking between the girders will experience moment. Tension controlled the transverse joints due to the negative moment in the girder (such as a negative moment over a pier); consequently the joints were tested in pure tension. The type of connection to resist these forces was investigated by Sam Lewis (2009). Lewis tested u-bar and headed bar connections (shown in Figure 2 and Figure 3, respectively) in order to determine which connection performed better. Performance was dependent upon strength, ease of construction, ductility, and cracking. (Lewis 2009)

Strain gauges were placed on the reinforcement in the in-situ joint zone shown in

Figure 4 and Figure 5. LVDT's were placed at the in-situ joint zone and at both ends to measure the deflection of the specimens. The transverse joint specimens were vertically placed in a frame and loaded to produce tension in the specimen until failure. (Lewis 2009)

The tensile capacities of the u-bar and headed bar were 414.7 kN (93.24 kips) and 408.2 kN (91.78 kips), respectively. The u-bar specimens also experienced more ductility. During construction it was found that the u-bar joint detail was easier to tie and set in place. The u-bar detail was also found to be less congested than the headed bars which would allow easier deck placement. Lewis (2009) concluded that the u-bar detail should be further considered for the in-situ joint connection. (Lewis 2009)

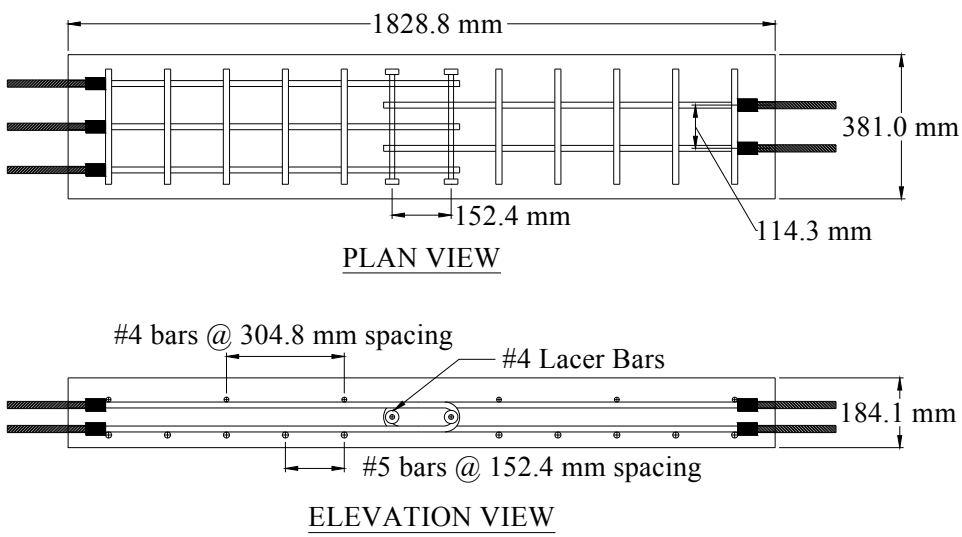

Figure 2: U-bar transverse joint

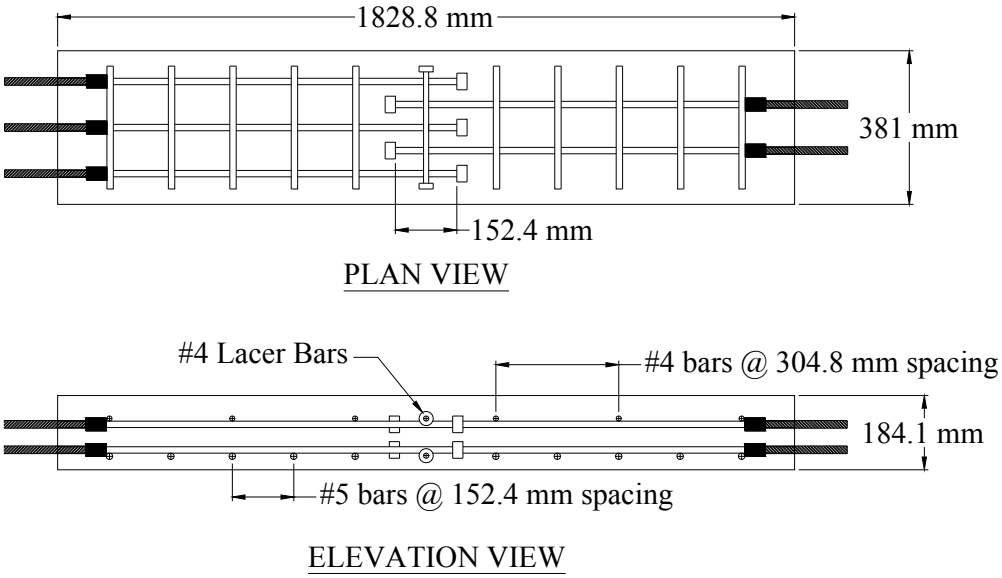

Figure 3: Headed bar transverse joint

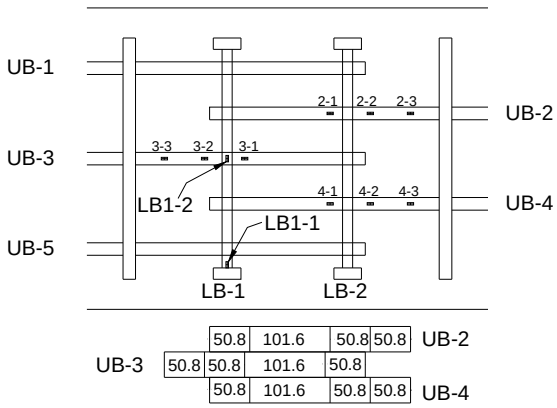

Figure 4: U-bar joint detail strain gauge configuration

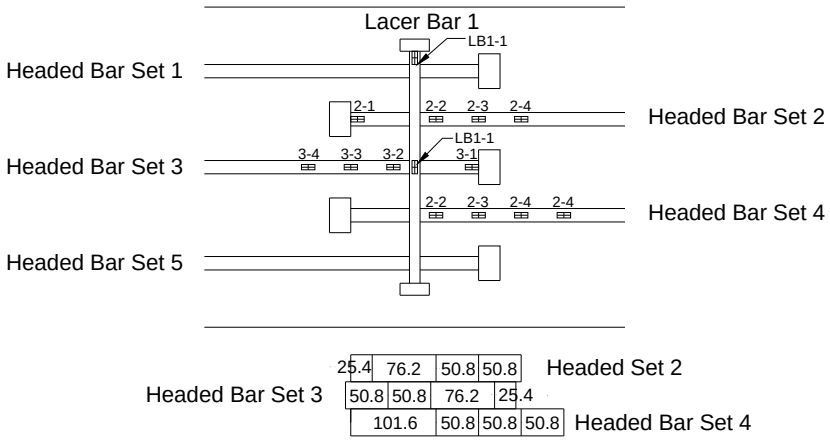

Figure 5: Headed Bar joint detail strain gauge configuration

Once the u-bar was selected for further testing, Beth Chapman (2010) produced more specimens to test in bending and tension. Figure 6 shows the tensile specimens' dimensions and reinforcement layout. In order to further understand the function of the u-bar joint connection in tension, three different parameters were considered: joint overlap length, u-bar spacing, and concrete compressive strength (values are shown in Table 1). Three different specimens were tested in tension. WT-4, shown in Figure 7, had a different width of 508 mm (20 inches) instead of 381 mm (15 inches) for the other specimens. Strain gauges were configured similar to Sam Lewis' configuration of the u-bars and lacer bars. (Chapman 2010)

The testing results, shown in Table 1, demonstrate that by increasing the u-bar spacing to 152.4 mm (6 inches) from 114.3 mm (4.5 inches) the capacity of the specimen increased approximately fourteen percent. If the joint overlap length is decreased to 101.6 mm (4 inches) from 152.4 mm (6 inches) then there is a decrease of approximately twenty three percent. Finally, if there is a decrease in the concrete compressive strength, then there will be a decrease in the specimen's capacity

dependent upon the concrete compressive strength. (Chapman 2010)

Peng Zhu (2010) completed testing of four different specimens for static test (represented by ST in Table 1) and fatigue tests (represented by FT in Table 1). The specimens consisted of the same dimensions and reinforcement layout (shown in Figure 6), as well as the same u-bar spacing and joint overlap length (shown in Table 1). Two panels were poured first and after the panels' concrete cured, the in-situ joint zone was poured to connect the panels. The in-situ concrete compressive strength and tested capacities are shown in Table 1 which provides similar results to Chapman's specimens with respect to the concrete compressive strengths. (Zhu 2010)

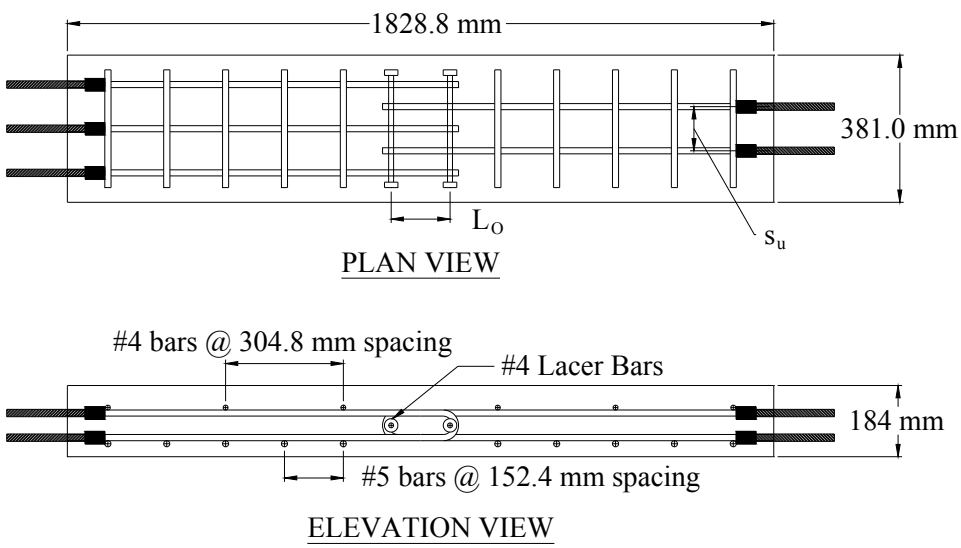

Figure 6: Tensile specimens WT-1, WT-2, WT-3, ST-0, ST-7, FT-0, and FT-7 with varying parameters shown in Table 1

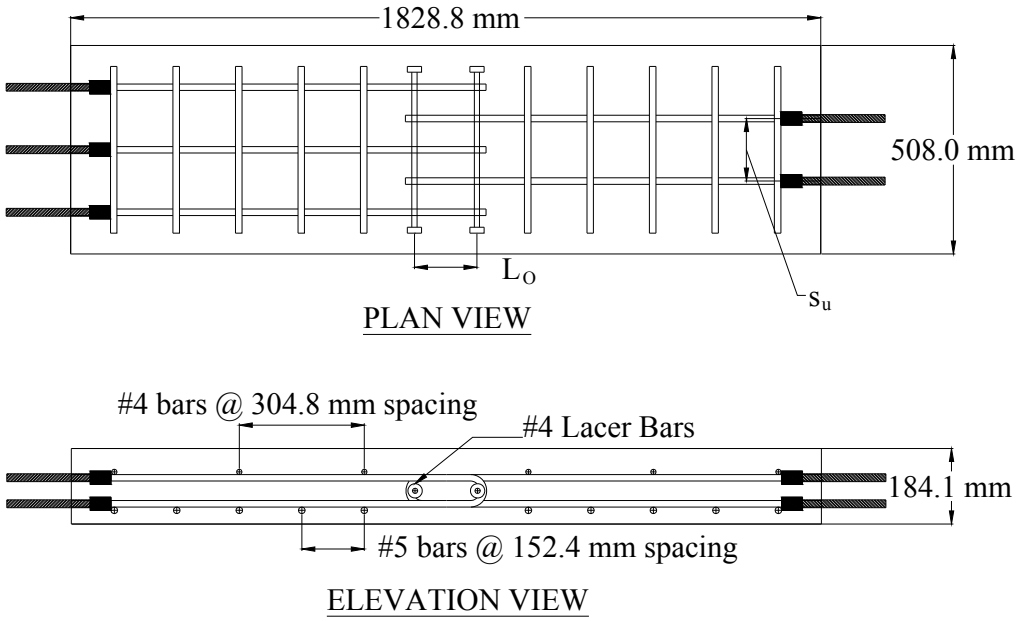

Figure 7: Tensile specimen WT-4 with parameters shown in Table 1

Table 1: Testing parameters and capacities of tensile specimens

	f'_c		U-Bar Spacing (s_u)		Joint Overlap Length (L_o)		F_{TESTED}	
Specimen	*(Mpa)*	*(psi)*	*(mm)*	*(in)*	*(mm)*	*(in)*	(kN)	(k)
WT-1	66.1	9582	114.3	4.5	152.4	6	414.55	93.20
WT-2	53.2	7719	114.3	4.5	152.4	6	394.54	88.70
WT-3	65.5	9496	114.3	4.5	101.6	4	336.27	75.60
WT-4	66.0	9576	152.4	6	152.4	6	474.16	106.60
ST-0	32.1	4656	114.3	4.5	152.4	6	301.57	67.8
ST-7	68.8	9979	114.3	4.5	152.4	6	415.96	93.5
FT-0	34.3	4975	114.3	4.5	152.4	6	289.97	65.2
FT-7	65.5	9500	114.3	4.5	152.4	6	449.96	101.2

1.3 Literature Review

Further testing of similar connections have been done by Gordon and May (2005) on the following five different types of specimens: Group A – Non-symmetrical looped bars with a central confined core of concrete with transverse bars (known in this paper as lacer bars), Group B – Non-symmetrical looped bars with a central

confined core without transverse bars, Group C – Symmetrical arrangements of looped bars with a central confined core, Group D – Symmetrical arrangements of straight lapped bars, and Group E – Symmetrical arrangements of hooked bars ending in the in-situ concrete joint zone. Group C is the most similar to the testing done by the University of Tennessee, but a variety of information from the other groups is relevant towards determining problems with these types of decking connections. (Gordon, S. R., et al. 2005)

Testing results for group A revealed the 8 mm lacer bars deforming severely in the post-yield stage which highlighted the importance of the lacer bar in the joint connection. When the diameter was increased from 8 mm to 16 mm the lacer bars deformed much less and provided more ductility beyond yielding. However, there still was noticeable deformation in the 16 mm diameter lacer bar at the ends. The predicted values for group A proved to be too high compared to testing, mostly due to the non-symmetrical arrangements of looped bars. Though the University of Tennessee's specimens were all symmetrical, the importance of the lacer bar, shown in Group A, cannot be overemphasized. (Gordon, S. R., et al. 2005)

Group B behaved similar to group A up to a certain load, and then a "sudden failure occurred." (Gordon, S. R., et al. 2005)) Transverse reinforcement was not present in group B; therefore, a brittle failure resulted without lacer bars in the specimens. (Gordon, S. R., et al. 2005)

Group C was most similar to the specimens tested at the University of Tennessee with the exception of the lacer bar configuration. Within the joint zone the researchers were able to place more transverse reinforcement which further confined

the in-situ joint zone. Group C specimens failed from either fracture or yielding of the longitudinal reinforcement. Several of the crack widths exceeded the British standard requirements in the in-situ joint zone. The largest of these cracks occurred at the end of the loops, while diagonal and splitting cracking was noticed at the center of the in-situ joint sections. Specimen T16 experienced a sudden failure due to the fracture of the lacer bar. along with diagonal cracking across the central concrete core. A bending shape of the lacer bar was noticed when smaller diameters were used (8 mm); however, when the larger lacer bars (16 mm) were utilized, the resulting shape remained straight. (Gordon, S. R., et al. 2005)

The previous examples demonstrate the importance of the lacer bar given that, when an adequate lacer bar is used, then the longitudinal reinforcement will control, resulting in a more ductile failure. The following statements from the paper further emphasize the function of the lacer bar "…the inclusion of adequate lacer bars is essential to prevent premature failure of the core by local crushing and splitting." "…the lacers have to be sufficiently robust to transfer the high local bearing stresses from the main looped bearing stresses from the main looped bars onto the central core concrete…" (Gordon, S. R., et al. 2005)

Ong, Hao, and Paramasivam (2006) proposed a strut and tie model to determine the ultimate tensile capacity for looped decking joint connections. Utilizing the current code computations proved to insufficiently calculate the capacity while other methods found were "…too elaborate and make use of many empirical coefficients." Two different types of specimens were tested: one with transverse cottering (known in this paper as lacer bars) reinforcement, and the other without transverse cottering

reinforcement. The specimens containing the transverse reinforcement provided a higher tensile capacity than those without. Two formulas were developed: one to determine the capacity of the specimen with transverse reinforcement and the second to determine the capacity without transverse reinforcement. Both formulas incorporated the spacing of the reinforcement. Design parameters were not given for the transverse bars; instead an empirical formula was used to reduce the connection capacity by twenty percent if no cottering reinforcement was provided. It was also found that the width of the strut was dependent upon the compressive strength of the in-situ concrete. The calculation proved comparable to the testing and provided more reasonable results compared to other previous methods of calculations. (Ong K. C. L., et al. 2006)

H.-K. Ryu et al. (2005) tested the cracking of a steel and concrete composite girder in flexure with a loop connection joint in the center of the span. The girder was tested in bending such that the concrete deck would be in tension. Testing showed that the reinforcement ratio and longitudinal reinforcement diameter did not significantly influence the cracks. Cracking, however, was observed above the transverse reinforcement and therefore was determined to be influenced by the transverse reinforcement. The authors reasoned that, if the deck is not prestressed concrete, then the formation of the cracks should be allowed, but the widths should be limited. The limitation appeared to be influenced by the transverse reinforcement thus the authors advised determining the influence of the transverse reinforcement. (H.-K. Ryu et al. 2005)

Chapter 2 Strut and Tie Modeling

2.1 STM for the joint connections

Through testing, researchers have observed a triangular formation of the concrete core in the in-situ joint section and have proposed using the strut and tie modeling method to design the joint zone (Chapman 2010, Lewis 2009). The strut and tie modeling method incorporates the compressive strength of concrete, called a strut, and the tensile strength of the rebar, called a tie. Due to the concrete and rebar interaction the forces will flow in such a way that a model can be developed. Upon simple observation the in-situ joint zone forms a truss shape which naturally is the idealized use for strut and tie modeling.

2.2 ACI strut and tie modeling

ACI 318-08 gives strut and tie modeling design criteria in Appendix A (ACI 318-08). Figure 8 demonstrates how a truss model can be formulated utilizing the lacer bar and u-bar spacing. The applied loads at the u-bar are given from the ultimate loads found in testing divided by the number of u-bars applying the load. There is equilibrium of forces in the model since the sum of the forces on both sides equals the ultimate capacity. The outer triangles, represented by the dashed lines, are considered zero bars in the model given that if the method of joints is used at point G the force in strut AG and tie GB are zero. In order to provide an example, the u-bar spacing, joint overlap length, and concrete compressive strength of Specimen WT-1 are applied to Figure 8. The maximum forces flowing through their respective joints are calculated by the method of joints provided in Table 2.

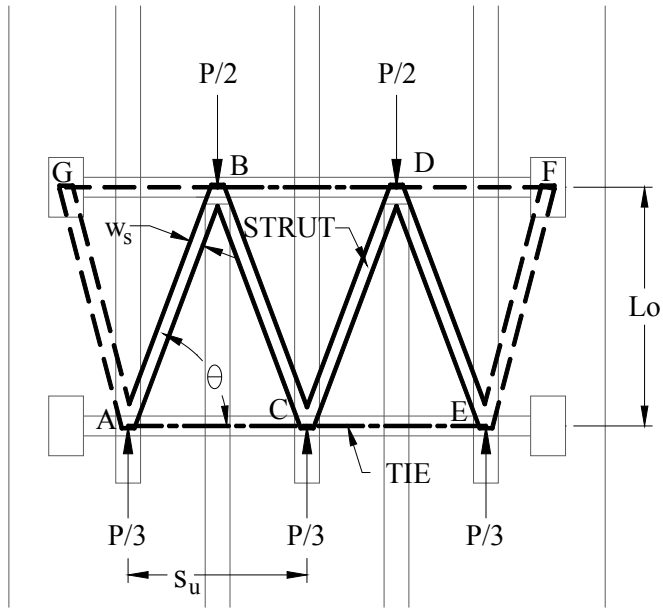

Figure 8: STM of joint section

Table 2: Maximum forces in their respective joints

Joints	Strut		Tie	
	(kN)	(k)	(kN)	(k)
A	147.58	33.18	51.83	11.652
B	147.58	33.18	0	0
C	73.79	16.59	51.83	11.625
D	147.58	33.18	0	0
E	147.58	33.18	51.83	11.625

Following ACI STM design the capacity of the struts, ties, and nodes must be greater than the forces flowing through them (ACI 318-08). The lacer bar is calculated without considering a reduction factor as follows:

$$F_{\mathrm{n}} = f_{\mathrm{y}} A_{\mathrm{b}} = 413.68\ MPa\ \times 129.032 mm^2\ = 53.38\ kN\ (12\ kips)$$

From the calculation the lacer bar used in the analysis is sufficient according to the model. However, if the capacity is checked with the reduction factor, the design would not be greater than the applied force in the model.

The capacity of the strut given from ACI 318-08 equations A-2 and A-3 is given as follows:

$$F_{ns} = f_{ce}A_{cs} = 0.85\beta_s f'_c A_{cs} \qquad \text{Eq. 2-1}$$

According to A.3.2.1, β_s may be taken as 1.0 which states that the strut is uniform over the entire length (ACI 318-08 A.3.2.1). The area of the strut (A_{cs}) is determined by the boundaries given to the node. As can be seen in Figure 8 the lacer bar is loaded by the u-bar resulting in a length of 15.875 mm (0.625 inches, the diameter of the u-bar), from this geometry the width of the strut (w_s) can be determined. The height of the strut is simply the depth of the inner diameter of the u-bar which is 47.625 mm (1.875 inches). The width of the strut is given by:

$$w_s = \frac{d_{\text{u-bar}}/2}{\sin(\theta)}$$

$$w_s = \frac{15.875\ mm/2}{\sin(69.44°)} = 8.477\ mm\ (0.33375")$$

The capacity from ACI strut and tie modeling can be determined without considering a reduction factor since this is not a design check:

$$F_{ns} = 0.85\beta_s f'cA_{cs}$$

$$F_{ns} = 0.85 \times 1.0 \times 66065\ kPa \times 8.477\ mm\ \times 47.625\ mm$$

$$F_{ns} = 22.67\ kN\ (5.097k)$$

This capacity is not greater nor equal to the forces in the strut from Table 2. For this joint zone the strut and tie modeling method given by ACI 318-08 is not sufficient for determining the capacity. The method is simplified making many assumptions in the in-situ joint zone that are not correct as the following statements demonstrate. The concrete core does not only utilize the concrete in the form of a strut but uses all of the concrete in the in-situ joint zone for additional strength (not represented in STM). The lacer bars in the STM are assumed to be in tension.

From the design above this assumption gives a reasonable value for the capacity shown in Table 2. However, the lacer bars observed from testing experienced excessive bending deformation and therefore the following conclusions can be made. The simplified assumption of the lacer bars acting in tension is wrong and the STM method does not give accurate design criteria for determining the capacity of the lacer bar. If the strut and tie modeling method is to be used for the joint zone then a modification must be made.

2.3 AASHTO strut and tie modeling

AASHTO also provides STM design specifications in section 5 of concrete structures. AASHTO differentiates itself from ACI in equation 5.6.3.3.3-1 (AASHTO 2007). This equation takes into account the tensile strain of the concrete from the tension tie in equation 5.6.3.3.3-2 (AASHTO 2007). However, the lacer bar does not undergo uniform tension but instead experiences excessive bending deformation (the lacer bar will be discussed in section 3.2). Therefore, the tensile strain in the concrete at the tension tie is assumed to be zero. If the tensile strain is not zero a value then a concrete compressive strength less than 0.85f'c would be used, therefore, using 0.85f'c is the maximum that could be used for the calculation. From this assumption the compressive concrete stress is then limited to 0.85f'c, resulting in the same strut capacity as the ACI STM design specifications.

2.4 Adjusted joint strut and tie model

Using STM design methods developed by ACI 318-08 and AASHTO specifications does not produce reasonable results, since these designs are not specific for this type of connection. The core of the concrete in the in-situ joint is not fully

utilized in STM calculations. If STM is to be used, then something must be corrected to fully utilize the concrete core and provide more accurate capacity calculations. Hawkins et al. (2005) mention using the depth of a beam with the angle of the strut to the tie to find the width of the strut. While the concrete core is not a deep beam nor the angle between the strut and tie 45° or less (as is the criteria from Hawkins et al. (2005)), this idea may be utilized in the strut capacity calculations in order to give a larger strut area and therefore a larger capacity to be more comparable to testing values. Figure 9 shows the width of the strut which better utilizes the concrete in the in-situ joint zone.

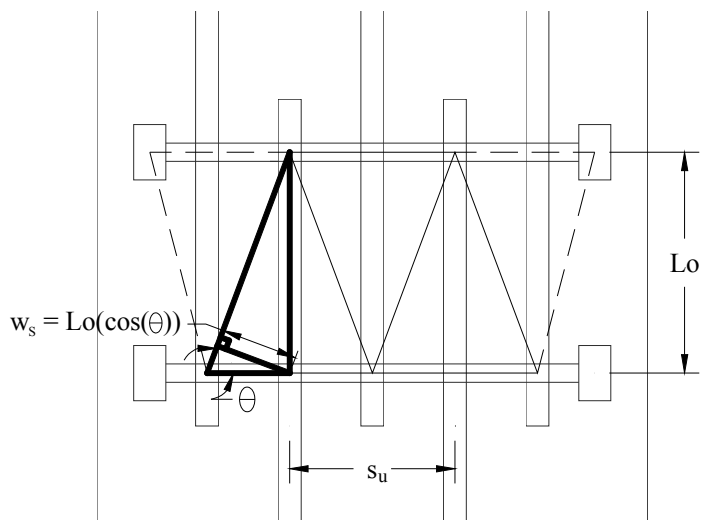

Figure 9: Width of the strut

From the same model in Figure 8 a new capacity may now be calculated from the new area. The width of the strut may be given as:

$$w_s = L_o \times cos\theta \qquad \text{Eq. 2-2}$$

$$w_s = 152.4\ mm \times \cos(69.44°) = 53.52\ \text{mm}\ (2.107")$$

The height of the strut is simply the inner radius of the u-bar given as 47.625 mm (1.875 inches) since the concrete core is confined in this depth by the u-bars. The capacity is calculated as follows:

$$F_{\text{ns}} = 0.85 f'_{\text{c}} A_{\text{cs}}$$

$$F_{\text{ns}} = 0.85 \times 66065\ kPa\ \times 53.52\ mm\ \times 47.625\ mm$$

$$F_{\text{ns}} = 143.13 kN\ (32.18k)$$

This calculated capacity is close to the maximum force in the STM and may be considered as a possible calculation for the capacity of the in-situ joint zone.

Table 3 shows the specimens' capacity calculated by using the adjusted strut width, as well as, the percent difference in the calculated capacity verses the model's maximum force. The model used in Table 3 is represented in Figure 8 with the applied forces acquired from the ultimate capacity from testing and the model's parameters (u-bar spacing, joint overlap length, and concrete compressive strength) determined by the respective specimen. The capacities are comparable with the exception of the decrease in the concrete compressive strength. The capacities are also represented in Figure 10 which shows a graph of the tested capacities verses the calculated capacities based on the concrete compressive strength. Any point above one on the vertical axis is considered conservative; therefore when the compressive strength decreases the capacities may become very conservative depending on the reduction in concrete compressive strength. Once the concrete compressive strength reaches approximately 68947.57 kPa (10,000 psi) the trend line reaches one on the vertical axis signifying that the calculation is equal to the tested value.

Table 3: STM calculated capacity verses testing

Specimen	f'c		U-Bar Spacing		Joint Overlap Length		Calculated Capacity of Strut		STM Forces from Testing		% Difference in Calc. vs Actual
	MPa	*psi*	*mm*	*in*	*mm*	*in*	*kN*	*kips*	*kN*	*kips*	
WT-1	66.1	9582	114	4.5	152.4	6	143	32.17	147.6	33.2	3%
WT-2	53.2	7719	114	4.5	152.4	6	115.3	25.92	140.5	31.6	18%
WT-3	65.5	9496	114	4.5	101.6	4	132.0	29.68	128.6	28.9	-3%
WT-4	66.0	9576	152	6	152.4	6	182.1	40.95	176.7	39.7	-3%
ST-0	32.1	4656	114	4.5	152.4	6	69.5	15.63	107.4	24.1	35%
ST-7	68.8	9979	114	4.5	152.4	6	149.0	33.5	148.1	33.3	-1%
FT-0	34.3	4975	114	4.5	152.4	6	74.3	16.7	103.2	23.2	28%
FT-7	65.5	9500	114	4.5	152.4	6	141.9	31.9	160.2	36.0	11%

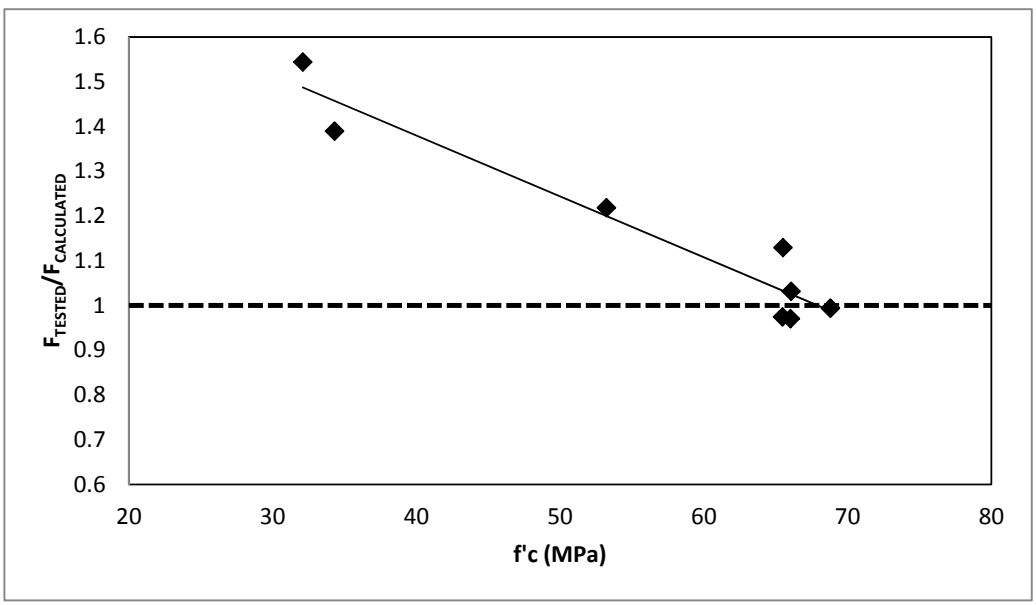

Figure 10: STM tested capacities verses calculated capacities based on f'$_c$

While the strut and tie model produces reasonable capacities with the widening of the strut, incorrect assumptions are made as the following state:

Strut and tie modeling assumes the forces flow through the model in such a way as to only produce tension and compression in the members; however, from testing

this assumption for the lacer bar is in incorrect. If the lacer bar is designed according to the strut and tie model then a number four rebar should be sufficient for the capacity as is evident in previous calculations from equation 1.1. However, from observation, the lacer bar of this size reaches a high plastic state which is not desired in design. As will be later shown, the lacer bar undergoes excessive bending deformation as is evident from observation after the testing and the lack of uniformity of the strain gauge readings from the lacer bars. If STM does not provide accurate modeling nor design for the lacer bar then another model must be used to provide accurate modeling and design.

Strut and tie modeling does not accurately model how the in-situ joint zone functions. As stated before, the outer struts in the model, struts AG and EF, have no forces going through them, however, this is incorrect. This section of the concrete core is obviously important as there are forces flowing from A to G and concrete must be in this zone otherwise the in-situ joint will not reach capacity. The concrete within the dashed triangles of Figure 8 must be accounted for in design.

According to the model shown in Figure 8 there are no forces acting on the top lacer bar represented in Table 2 by points B and D. From testing, however, there is deformation in both of the lacer bars therefore a conclusion can be made that this model is not accurate for the top lacer bar. Even if the design of the bottom lacer bar is used the designer would not know if the top lacer bar controls due to the fact that there is different loading scenarios on both of the lacer bars.

The new design method for determining the capacity of the in-situ joint zone must be able to model the joint zone correctly, determine an accurate capacity, and design the lacer bar appropriately.

Chapter 3 Triangular Method

3.1 Tension Joint Capacity Calculations

The joint detail ultimate strength calculations are based on observations during loading and failure from Sam Lewis' paper (Lewis 2009) and from specimens examined after failure. The following picture reveals the basic concept in the calculations (Figure 11).

Figure 11: Concrete triangular formation

The triangular shapes within the photo signify the failure in the concrete of the transverse joint specimen. The concrete center triangle remains intact which helps to illustrate how the forces are transferred through the concrete. The loaded area (A_L) at the radius of the u-bar for the concrete center triangle is obviously taken from a combination of the u-bar and the lacer bar as is evident in the picture. The force flows from the u-bar to the loaded area and is then distributed directly to the bearing area (A_B). The bearing area shall be defined as the area of concrete which bears on the lacer bar and u-bars on either side of the u-bar applying the load, as a reaction to the applied load of the u-bar; therefore, one of the strength parameters of the concrete

shall be the bearing of the concrete (F_B).

The geometry of the triangle should compose of the u-bar spacing and lacer bar spacing as is shown in joint zone in Figure 12. In using the joint zone of Figure 12 as a reference, the length shall be the inner edge of the lacer bars of the overlap length. A line going from the inside radius of the opposing u-bars intersects the lacer bars which gives the width of the triangular specimen.

Sam Lewis (2009) noted that the transverse specimen would crack in the transverse direction above the lacer bar first (Lewis 2009). Londgitudinal cracking would then occur between the transverse cracks and failure would occur when the longitunial cracks would reach the transverse cracks (Lewis 2009). From Lewis' cracking observations and the free body diagram, shown in Figure 12, there is a tensile strength (F_T) and a shear strength (F_V) of the specimen; however, a pre-cracking and post-cracking stage of the in-situ joint zone must be considered. The pre-cracking stage for the triangular concrete specimen is composed of the horizontal strengths of the tensile and shear strengths, but once the in-situ joint zone cracks (post-cracking), no more tensile strength can be developed. The ultimate strength is then dependent upon the shear strength. The post-cracking stage will only be considered since this calculation is for the ultimate capacity; therefore, the tensile strength will be understood to be zero. Once cracking has occurred, the shear strength can be developed from the interlocking of aggregate and the friction of the two interlocking faces of the opposing triangles.

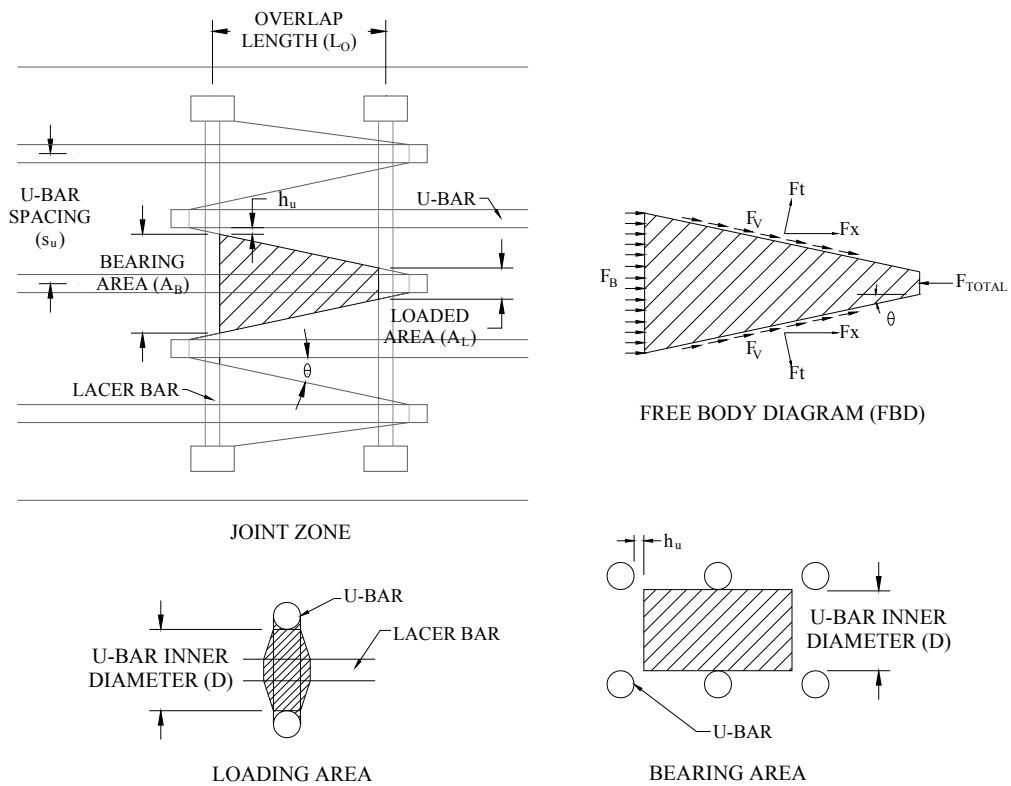

Figure 12: Triangular method

From the free body diagram in Figure 12 the following formula is proposed for calculating the capacity of the specimen:

$$F_{\text{TOTAL}} = n(F_{\text{B}} + F_{\text{x}}) \qquad \text{Eq. 3-1}$$

The "n" represents the minimum number of concrete triangles. F_x considers the horizontal shear strength of concrete. Within the formula is the assumption that the joint will fail once the concrete fails and therefore does not consider the failure of the u-bars and lacer bars. F_B represents the strength due to the concrete triangle bearing surface and is found using the following formula:

$$F_{\text{B}} = 0.85 f'_{\text{c}} A_{\text{L}} \sqrt{\frac{A_{\text{B}}}{A_{\text{L}}}} \qquad \text{Eq. 3-2}$$

f'_c – compressive strength of concrete in psi

A_L – Loaded Area of concrete (in^2)

A_B – Bearing Area of concrete (in^2)

The loaded area (A_L) shall be defined as the area of concrete which forms at the point of the triangle due to the applied load from the u-bar. A_L can be found from Figure 12 which shows that the loaded area is dependent upon the lacer bar and u-bar inner radius. The area at the lacer bar (Figure 12) is dependent upon the u-bar spacing and the angle (θ) shown in Figure 12. Therefore, the lacer bar area can be determined by equation 3-3:

$$A_{\mathrm{L}} = d_{\mathrm{UB}}D + d_{\mathrm{UB}}{}^2 - A_{\mathrm{UB}} + 2\mathrm{h_u}d_{\mathrm{LB}} + [D - d_{\mathrm{LB}}]\mathrm{h_u} \qquad \text{Eq. 3-3}$$

Figure 12 shows how A_B can be found which goes from the inner edges of the u-bars on either side of the u-bar applying the load to the assumed triangular concrete section. The bearing area (A_B) can be calculated by the following formula:

$$A_{\mathrm{B}} = D[(s_{\mathrm{u}} - d_{\mathrm{UB}}) - 2\mathrm{h_u}] \qquad \text{Eq. 3-4}$$

$\sqrt{\frac{A_B}{A_L}}$ in Equation 3-2, represents the confinement due to the surrounding concrete and is taken from 10.14 of ACI 318-08. According to 10.14 the surrounding concrete confines the bearing area which increases the bearing strength (R10.14.1) but this is limited to 2 (ACI 318-08 10.14), however, no limitation is given to this calculation since there is also confinement from the lacer bars and u-bars. Another limitation is that the supporting area must be wider than the loaded area on all sides. This limitation is not applied to the confinement calculation since the height is determined by the u-bar inner radius.

The shear strength in the horizontal-direction is taken as:

$$\mathrm{F_{Vx}} = 2\left(2\lambda\sqrt{\mathrm{f'_c}}\mathrm{A_v}\right)cos\theta \qquad \text{Eq. 3-5}$$

$$\mathrm{A_V} = \frac{(\mathrm{L_o} - \mathrm{d_{LB}})}{\cos\theta}\mathrm{h_{slab}} \qquad \text{Eq. 3-6}$$

The shear strength of the concrete is taken from equation 11-3 from 318-08 ACI representing a lower bound for shear. The "2" is for the two sides of the triangle shown in the free body diagram in Figure 12. "h_{slab}" is the height of the concrete slab. Upon substituting equation 3-6 for A_V into equation 3-5 the following formula can be obtained:

$$F_{Vx} = 4\lambda\sqrt{f'c}(L_o - d_{LB})h_{slab} \qquad \text{Eq. 3-7}$$

Specimen WT-1 is shown in

Figure 13 and had a 28-day compressive strength of 66065.56 kPa (9582 psi), a u-bar spacing of 114.3 mm (4.5 inches), and a joint overlap length of 152.4 (6 inches). From these parameters the capacity of specimen WT-1 may be calculated.

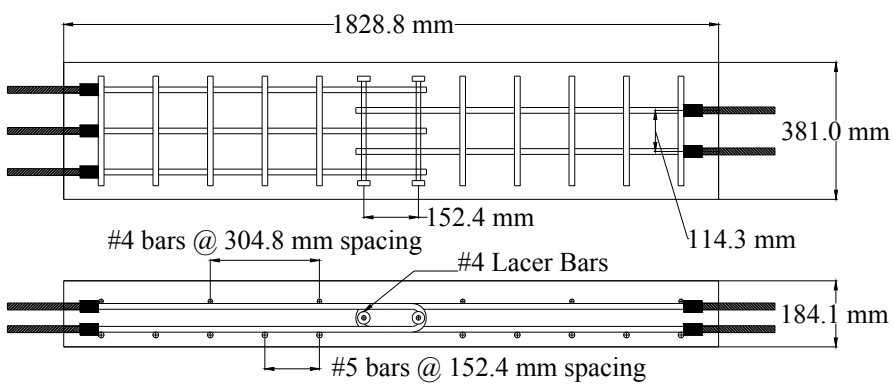

Figure 13: U-bar transverse joint specimen

From Equation 3-3 the loading area can be calculated:

$$A_L = 15.875\ mm \times 47.625\ mm + (15.875mm)^2 - 200mm$$

$$+ 2\times 6.21\text{mm}\times 12.7mm + [47.625\ mm - 12.7\ mm]\times 6.21\text{mm}$$

$$A_L = 1182.68\ mm^2\ (1.83\ in^2)$$

From Equation 3-4 the bearing area can be calculated:

$$A_B = 47.625\ mm[(114.3\ mm - 15.875\ mm) - 2 \times 6.21\text{mm}]$$

$$A_{\mathrm{B}} = 4095.99\ mm^2\ (6.349in^2)$$

Therefore, from Equation 3-2 the capacity from the concrete bearing on the lacer bars and u-bars (F_B) can be found:

$$F_{\mathrm{B}} = 0.85f'cA_{\mathrm{L}}\sqrt{\frac{A_{\mathrm{B}}}{A_{\mathrm{L}}}}$$

$$F_{\mathrm{B}} = 0.85 \times 66.1MPa \times 1182.58mm^2 \times \sqrt{\frac{4096.12mm^2}{1182.58mm^2}} = 123.6kN$$

The shear capacity from equation 3-7 may also be determined:

$$F_{\mathrm{Vx}} = 4 \times 1 \times 674.9kPa \times (152.4mm - 12.7mm) \times 184.1mm = 69.45kN$$

The capacity of the assumed concrete triangle can be found from equation 3-1:

$$F_{\mathrm{TOTAL}} = 2 \times (123.6kN + 69.45kN) = 386.1kN$$

Table 4 shows the calculated capacity of the triangular concrete specimens compared to the tested capacity. A positive percent difference in the calculated verses tested capacities indicates that the calculated value is less than the tested. The different variables in the specimens have been highlighted to emphasize the difference of the specimens being tested. The table shows that the capacity of the triangle changes as the variables change (f'c, u-bar spacing, and joint overlap length) without having to change or add any parameters within the calculations.

Table 4: Calculated verses tested capacities dependent upon different variables

Triangular Method											
Specimen	f'c		U-Bar Spacing		Joint Overlap Length		Capacity of Specimen		F_{ACTUAL}		% Difference in Calc. vs Actual
	MPa	*psi*	*mm*	*in*	*mm*	*in*	*kN*	k	kN	k	
WT-1	66.1	9582	114.3	4.5	152.4	6	386.1	86.8	414.6	93.2	7%
WT-2	53.2	7719	114.3	4.5	152.4	6	323.8	72.8	394.5	88.7	18%
WT-3	65.5	9496	114.3	4.5	101.6	4	340.3	76.5	336.3	75.6	-1%
WT-4	66.0	9576	152.4	6	152.4	6	449.1	101.0	474.2	106.6	5%
ST-0	32.1	4656	114.3	4.5	152.4	6	216.9	48.8	301.6	67.8	28%
ST-7	68.8	9979	114.3	4.5	152.4	6	399.1	89.7	416.0	93.5	4%
FT-0	34.3	4975	114.3	4.5	152.4	6	228.4	51.4	290.0	65.2	21%
FT-7	65.5	9500	114.3	4.5	152.4	6	383.4	86.2	450.0	101.2	15%

Figure 14 represents the calculation verses actual failure (y-axis) depending on the concrete compressive strength (x-axis). Any Tested/Calculated value (y-value) above one is considered conservative. Most cases are slightly conservative with the exception of specimen WT-3 which has a value of 0.99, representing a valid calculation theory for this specimen.

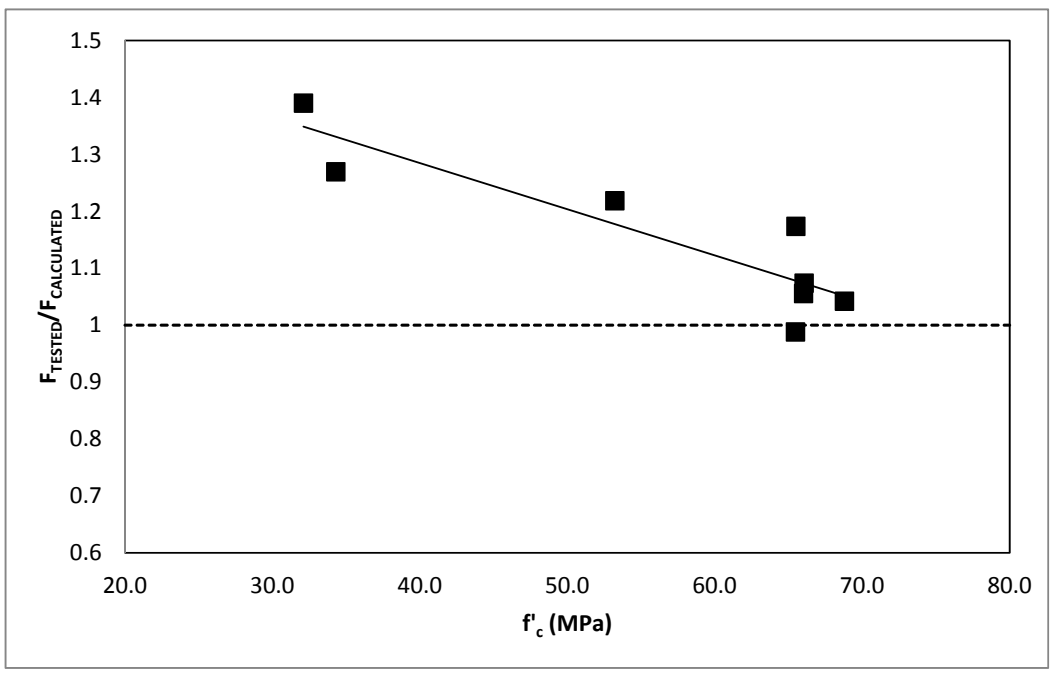

Figure 14: Triangular Method calculated verses tested capacities based on f'$_c$

The trendline in Figure 14 represents the how the concrete compressive strength affects the calculated capacity. As the concrete compressive strength is below 68947.57 kPa (10,000 psi) the calculated capacity of the assumed concrete triangle becomes more conservative. However, according to the trendline, if the concrete compressive strength is equal to approximately 68947.57 kPa (10,000 psi) or greater then the concrete triangular method is no longer considered conservative (this would require testing specimens greater than 68947.57 kPa (10,000 psi) for confirmation). An option to consider enforcing in design would be to limit the triangular method to 68947.57 kPa (10,000 psi) concrete. This would also maintain consistency with ACI 318-08 in limiting the $\sqrt{f'_c}$ to 689.5 kPa (100 psi) (ACI 318-08 11.1.2). By limiting the concrete compressive strength to 68947.57 kPa (10,000 psi) the calculated capacity would then be approximately equal to the actual value or more conservative for a concrete compressive strength less than 68947.57 kPa (10,000 psi).

3.2 Lacer Bar

Previous research has not provided sufficient information about the lacer bar. Most researchers understand that it allows the joint zone to be more ductile as there have been many tests which show the joint zone is brittle without the lacer bars (Gordon et al. 2005). The strain gauge configuration on the lacer bar of Sam Lewis' (2009) and Beth Chapman's (2010) research assumes the lacer bar acts in tension. The test results, however, show the lacer bar acts in bending. Figure 15 and Figure 16 show common representations of the lacer bar strain gauge data in testing (Lewis 2009 and Chapman 2010). These figures do not demonstrate any uniformity in

tension and therefore, the lacer bar does not act in pure tension. Also, from simple observation the lacer bar undergoes excessive deformation due to bending as can be seen in Figure 11. Further observation of the deflection shows that the lacer bar deforms where the u-bar applies the force and where the lacer bar bears against the concrete. This observation would verify that force flows in the order of the following: The tensile force pulls the u-bar, the u-bar bears on the lacer bar, the lacer bar transfers the force to the concrete (the loaded area), the concrete distributes the force in a triangular pattern in the direction of the opposite lacer bar where the concrete bears against the lacer bar (bearing area).

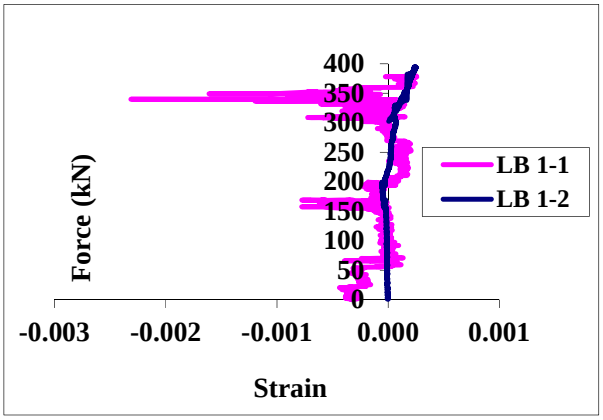

Figure 15: WT-2 Top of the Lacer Bar

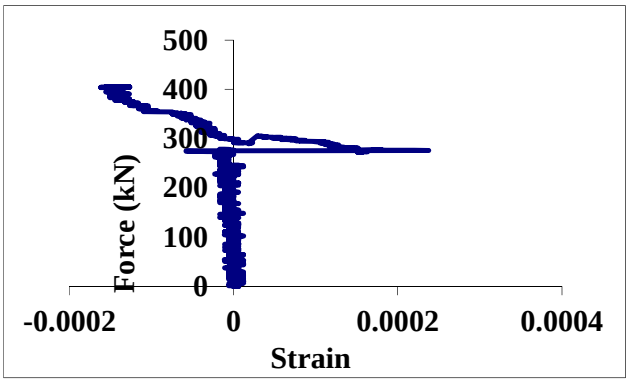

Figure 16: WT-4 Lacer Bar

The failure of the lacer bar should be carefully considered. The lacer bar allows ductility but also gives excessive cracking along the in-situ joint section which may not satisfy cracking and servicability requirements. Therefore, modeling the lacer bar would prove beneficial in understanding and assisting with the design of the lacer bar. The proposed trianglular method has been used to model the lacer bar. In order to model the lacer bar the following parameters and restraints were used: The length of the lacer bar is from center to center of the heads of the lacer bar. The ends are assumed fixed due to a tangent line of the deflected shape approximately perpendicular to the head and also due to the concrete surrounding the head on the inside of the lacer bar which mostly stays in tact after failure. There are three loads applied to the lacer bar as follows: firstly, the direct load from the u-bar taken as a uniformily distributed load for a distance equal to the diameter of the u-bar (ω_L), secondly, a uniformily distributed bearing load from the base of the concrete triangle (ω_B), and lastly, the bearing strength of the concrete as the lacer bar deflects and bears against the concrete from the u-bar loading (ω_{CONC}). The distributed loads may be determined as follows:

$$\omega_B = [P_{ULT} - n \times Fx] \times \frac{1}{N_B \times L_B} \qquad \text{Eq. 3-11}$$

$$\omega_L = \frac{P_{ULT}}{N_L \times d_{u\text{-}bar}} \qquad \text{Eq.3-12}$$

$$\omega_{CONC} = f'_c \times d_{lacerbar} \qquad \text{Eq. 3-13}$$

P_{ULT} – Capacity of the specimen

Fx – Minimum horizontal resistance provided by one concrete triangle from shear due to P_{ULT}

n – Minimum number of triangles for the specimen

N_B – Number of triangles bearing on the lacer bar

L_B – Length of the bearing area on the lacer bar

N_L – Number of triangles loaded by the u-bar

The bearing load (ω_B) is taken from the ultimate capacity minus the minimum horizontal capacity since the bearing on the lacer bar is not the only contribution of the concrete triangular strength as can be seen from Figure 12 of the FBD. From this figure some of the force is distributed to the core of concrete in the in-situ joint.

The bearing strength of the concrete (ω_{CONC}) is typically applied to one side of the lacer bar because the lacer bar tends to deflect in the same direction where the majority of the load is applied in the center as can be seen in Figure 17. For example, if two u-bars are contributing force to the lacer bar, as in Figure 18 and the bearing length is in the center, then the lacer bar will deform in the direction of the loading u-bars, not the bearing. In this case ω_{CONC} may be applied against the lacer bar on the opposite side of the loading u-bars in order to help resist the loading of the u-bar. However, if the reverse is true (the lacer bar is being loaded in the center and has a bearing force on opposite sides of the center shown in Figure 19), then ω_{CONC} is only applied against the loading of the u-bars on the ends. In this second case the lacer bar deforms away from the core of the in-situ joint zone which typically is cracked and cannot be assumed to be used to bear against. However, the concrete around the head of the lacer bars typically stays intact and may be used for additional bearing load (ω_{CONC}).

While these are general rules, the lacer bar can be modeled only using the loading and bearing loads as a start to the model. Once the direction and deflection of the

lacer bar is known then ω_{CONC} can be applied accordingly. Equation 3-13 is a limit for ω_{CONC} and provides a place to begin the analysis. Once ω_{CONC} is applied, if the lacer bar deflects in the opposite direction then too much of the bearing strength has been applied to the model (since the bearing strength is only meant as a reaction, not an applied load). ω_{CONC} may be decreased until a reasonable deflection is observed. A reasonable deflection is a deflection that has been observed in testing previously. For example, from specimen WT-1 the deflection at the center is approximately zero while specimen ST-0 experienced a deflection of 13.45 mm (0.5294 inches) at the u-bar location. These deflections would represent the range that could be applied to the analysis. If, for example, the loading and bearing loads produce a deflection of 12.7 mm (0.5 inch) then the designer should use engineering judgment when applying ω_{CONC}. The designer would know a deflection of zero would be allowed and that the bearing would cause the deflection to be reduced from 12.7 mm (0.5 inch). Therefore once the designer applies ω_{CONC} and if a deflection of 5.33 mm (0.21 inch) is produced then the moment and shear from the model could be used for designing the lacer bar.

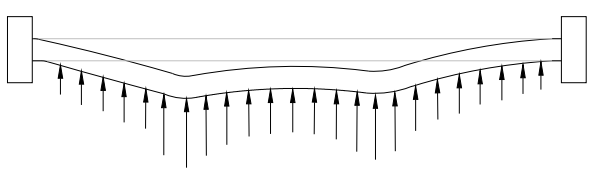

Figure 17: (ω_{CONC}) Concrete bearing reaction to the lacer bar deflection

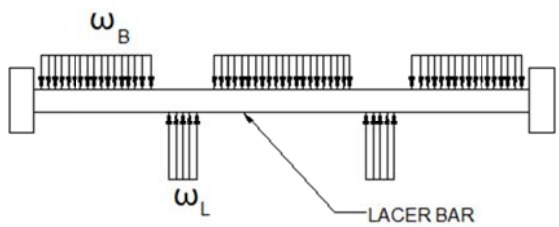

Figure 18: Loading configuration of the lacer bar where loading controls

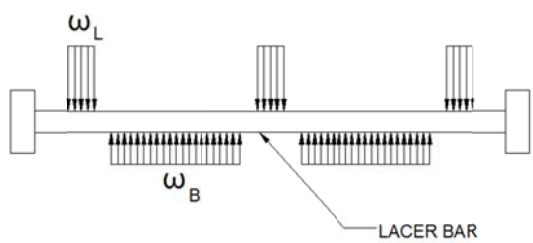

Figure 19: Loading configuration of the lacer bar where bearing controls

In order to further show how to model the lacer bar, specimen WT-1 will be modeled and analyzed. Figure 11 shows the deformation of the lacer bar being analyzed. The modeling parameters must first be identified: From previous calculations P_{ult} = 386.1 kN (86.8 k), Fx_{min} = 69.45 kN (15.6 k), L_B = 86 mm (3.386 in). From observation of the formation of the triangles, $N_B = 2$, $N_L = 3$, and n = 2. Therefore, the rest of the parameters may be calculated from equations 3-11, 3-12, and 3-13:

$$\omega_B = [386.1\ kN - 2 \times 69.45kN\ ] \times \frac{1}{2 \times 86mm}$$

$$\omega_B = 1.44\ kN/mm$$

$$\omega_L = \frac{393.43\ kN}{3 \times 15.875\ mm} = 8.11\ kN/mm$$

$$\omega_{CONC} \leq 66.1\ MPa \times 12.7\ mm = 0.839\ kN/mm$$

Figure 20, Figure 21, and Figure 22 show the placement of the distributed loads,

ω_L, ω_B, and ω_{CONC}, respectively, on the lacer bar depending upon the location of the u-bars being spaced at 114.3 mm (4.5 inches) for representation of specimen WT-1.

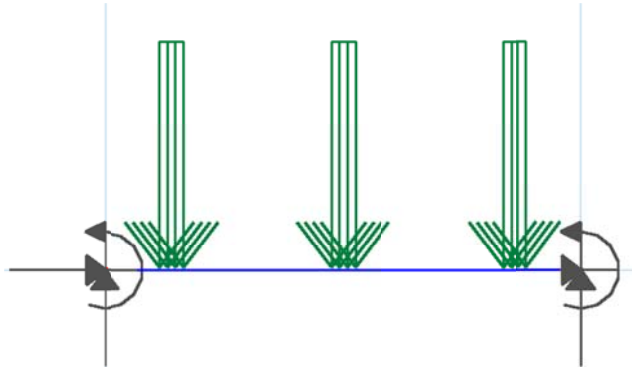

Figure 20: ω_L locations

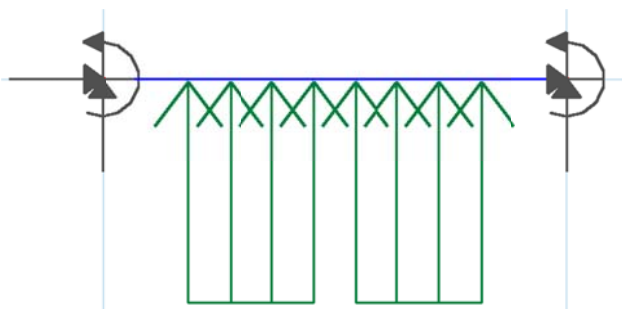

Figure 21: ω_B locations

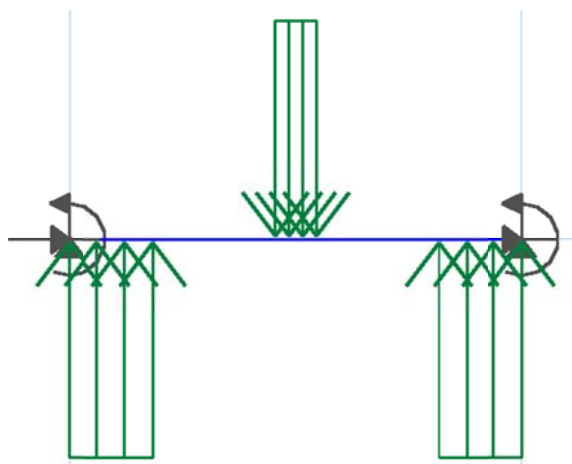

Figure 22: ω_{CONC} locations

According to Figure 11 the concrete at the heads of the lacer bar stay intact up

until the closest concrete triangle bearing point and therefore ω_{CONC} supports against the loading u-bars at the locations shown in Figure 22. The center triangle (shown in Figure 11) stays intact and is considered in tension as a distributed load along the loading length (u-bar diameter) of the triangle. Since the lacer bar will tend to deflect in the direction of where the majority of load is applied in the center then the lacer bar will deflect in the direction of the bearing forces (ω_{B}). However, in Figure 11 the lacer bar appears to not deflect in this direction and is being held back by the center triangle; therefore, the center triangle is represented in Figure 22 as the center load resisting the deflection. The tensile strength of concrete according to ACI 318-08 R10.2.5 is a variable property of concrete and is taken from ACI 318-08 18.4.1 to be $6\sqrt{f'c}$ (ACI 318-08 18.4.1). In this model the tensile capacity is then:

$$\omega_{\text{CONC}} = 6\sqrt{f'c} \times D = 6 \times 674.9kPa \times 47.625\,mm = 192.84\frac{N}{mm}$$

D is the diameter of bend of the u-bar. This tensile bearing strength is the ultimate that the triangle could provide. If this number is used then the bar deflects in the direction of tensile bearing capacity. However, this cannot be the case since the tensile strength is a reaction to the deflection. Therefore, the tensile bearing reaction was reduced to 36% of the tensile capacity so that there would be no deflection in the center of the lacer bar.

Figure 23 shows the deflected shape of the lacer bar (shown in red) once analyzed according to the model. In comparing the actual deflected shape (Figure 11) to the one being modeled (Figure 23) it appears they have similar points of inflection.

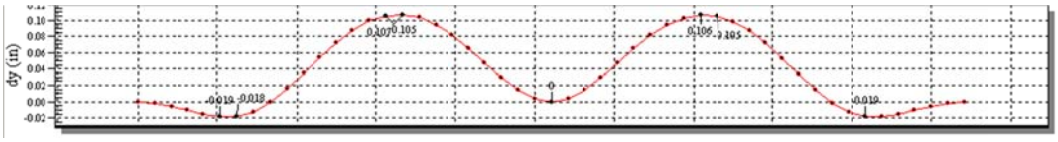

Figure 23: Deflected shape of the lacer bar according to the proposed model

The model gives a maximum deflection at the location of the two u-bar loading points of 2.72 mm (0.107 inches). The deflection at the center is 0 mm. The maximum moment in the lacer bar is at the center with a value of 1306 kN-mm (11.56 k-in). The lacer bar now has some design criteria being the maximum moment and shear from the model and the deflection at ultimate. The deflection is proportional to the crack widths. If the deflection (cracking) does not satisfy requirements then the lacer bar diameter must be increased or another bar added to decrease the deflection. However, the spacing of the lacer bar to the u-bar or another lacer bar must be checked with ACI 318-08 spacing criteria. It should also be noted that there are two sides to the specimen and both lacer bars need to be checked in order to determine the worst case deflection and moment.

Specimen ST-0's lacer bar is modeled below; however, in order to model the correct deflected shape from testing a few of the calculated loads on the lacer bar need to be adjusted. Figure 24 shows the lacer bar in question which is loaded similar to Figure 18 where the loading will control the direction of the deflection. In modeling the lacer bar according to the defined rules the deflected shape is as is shown in Figure 25. This loaded deflected shape is not exactly what is shown in Figure 24 and therefore a few adjustments must be made to account for the assumptions made. The middle bearing load (ω_B) changes from 0.465 kN/mm (2.658 k/in) to 0.525 kN/mm (3

k/in) and the concrete bearing strength (ω_{CONC}) changes from 0.408 kN/mm (2.328 k/in) to 0.482 kN/mm (2.75k/in). These corrections in the model are simply adjusted assumptions. The assumption of the bearing load is that some of the load is taken from the horizontal strength of the triangle. While this assumption is correct, according to the theory, the confinement is an approximated increase of the bearing strength. Also, the shear strength calculation, taken from ACI 318-08, is a conservative approximation of the triangular shear strength. Given the uncertainties in the concrete and lack of mathematical understanding of confinement and shear, the increase in bearing strength (ω_B) is reasonable so as it is not excessive. The bearing strength of the concrete (ω_{CONC}) is also increased since the calculated value is the minimum bearing strength and does not consider the confinement of the in-situ joint zone from the reinforcement and surrounding concrete.

Figure 26 represents the modeled deflection once the adjustments are incorporated, which is more similar to the actual deflected shape shown in Figure 24. The points of inflection of the adjusted model and the actual lacer bar are at the same locations and also have similar deflections. The actual maximum deflected shape is 13.45 mm (0.5294 inches) compared to the modeled deflection of 22.96 mm (0.904 inches) and the adjusted model deflection of 13.77 mm (0.542 inches).

The models may also be compared by their respective moments produced on the lacer bar. The modeled maximum moment is 1564.76 kN-mm (13.85 k-in) compared to 1313.9 kN-mm (11.63 k-in) from the adjusted model, resulting in a number 9 and number 8 rebar, respectively, if allowing plastic bending (design of the lacer bar will be discussed in Section 4.3).

Figure 27 shows the lacer bar compared to the adjusted model represented by the thick line in the figure. This specimen represents the validity of the lacer bar function but also represents the uncertainties of concrete in the model by presenting some of the unknown in how the loads are applied and calculated in the model. It should be noted that the modeling will also be affected by the calculated values used which vary depending on the concrete compressive strength, as is shown in Figure 14.

Figure 24: ST-0 lacer bar from loading side

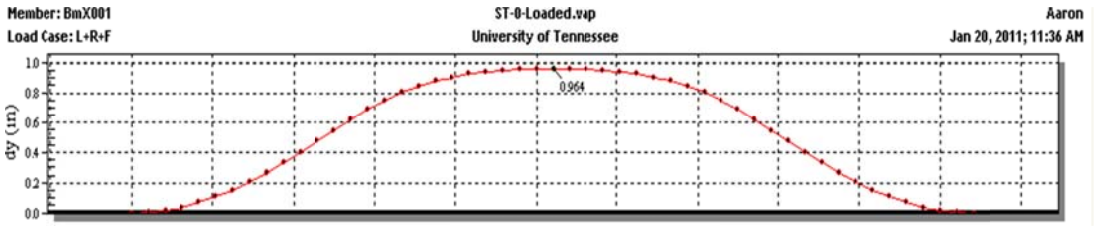

Figure 25: Deflected shape of lacer bar of specimen ST-0 according to rules given

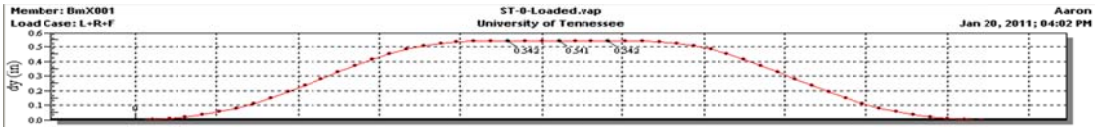

Figure 26: Deflected shape of lacer bar of specimen ST-0 according to the adjusted model

Figure 27: ST-0 lacer bar from loaded side compared to the adjusted model

Specimen ST-0's bearing lacer bar, shown in Figure 28, has been modeled similar to Figure 19. If the lacer bar is modeled as defined above then the deflected shape, shown in Figure 29, has a maximum deflection of 9.73 mm (0.383 inch), a maximum moment of 1116.2 kN-mm (9.88 k-in), and a maximum shear of 40.09 kN (9.012 k). The actual maximum measured deflection of the lacer bar is 4.23 mm (0.1665 inch). This model does not give the correct deflected shape, however, if the bearing load is increased to 0.77 kN/mm (4.4 k/in) from a calculated 0.698 kN/mm (3.987 k/in) and reanalyzed then the deflection is 4.17 mm (0.164 inch), shown in Figure 30. Figure 30 is an exaggerated deflected shape of the lacer bar and has the same points of inflection and a very accurate deflection.

The moments, shears, and required lacer bar diameters (design of the lacer bar will be discussed in Section 4.3) from the models are as follows: 1116.2 kN-mm (9.88 k-in), 40.09 kN (9.012 kips), and a number 8 rebar for the defined model; 939.9 kN-mm (8.319 k-in), 35.02 kN (7.873 kips), and a number 8 rebar for the adjusted model.

Figure 31 shows how accurate the adjusted model's deflection curve (shown by the thick line on the lacer bar) is compared to the actual lacer bar. This example

validates the method but reveals slight inaccuracies in the concrete calculations since the bearing load had to be increased to mirror the actual deflected shape. These inaccuracies are unknown mathematical characteristics of concrete and the required adjusted values vary from specimen to specimen. Also, the concrete bearing strength (ω_{CONC}) may not always be known as is the case in the loaded lacer bar from specimen ST-0.

Figure 28: ST-0 lacer bar from bearing side

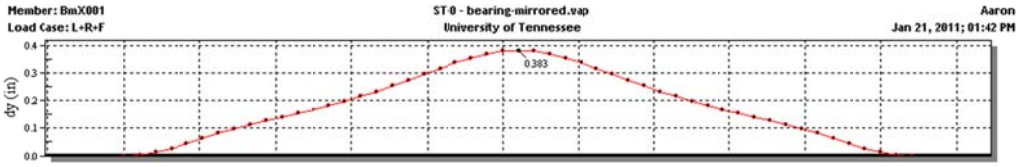

Figure 29: ST-0 lacer bar from bearing modeled as defined

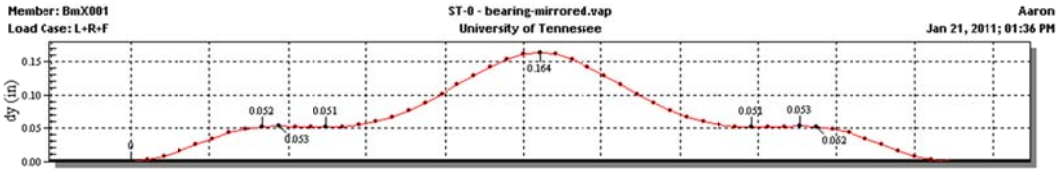

Figure 30: ST-0 lacer bar from bearing adjusted model

Figure 31: ST-0 lacer bar compared to the adjusted model deflection

Chapter 4 Recommended Design Criteria for the Triangular Method

The triangular concrete design method assumes the concrete in the in-situ joint zone will develop a triangle. This assumed triangle's capacity is calculated based on a free body diagram of one triangle taking the observed confinement of the in-situ joint zone into consideration. Section 3.1 develops how to calculate the capacity of the triangle but the following gives some design criteria which must be examined before a complete design method has been formulated. In order to determine the bearing strength, extensive area calculations are necessary to calculate the actual capacity.

It should be noted that this method calculates the capacity of the concrete in the in-situ joint zone, but this is not the only failure mode of the decking joint which must be checked. The objective of this calculation is to check for u-bar failure before the concrete joint failure since the u-bar will provide more ductility. The u-bar allowable tension and serviceability must be checked. In the in-situ joint zone the serviceability is related to how the lacer bar deforms, indicating that certain design criteria must be developed for the lacer bar.

4.1 Area Calculations of the Bearing Strength Capacity

Equation 3.1 gives the formula for calculating the triangular concrete strength using the FBD. From the FBD in Figure 12, there are only two parameters to consider: the bearing strength (F_B) and horizontal strength (F_X). The bearing strength equation is given in equation 3.2; however the loading area and bearing area

are very detailed. For design these areas need to be simplified and yet remain accurate, therefore two different calculations of the loaded area (A_L) and bearing area (A_B) shown below have been compared to the actual areas given in section 3.1. The following show Design 1:

$$A_{\mathrm{L}} = d_{\mathrm{UB}}D + d_{\mathrm{UB}}{}^2 - A_{\mathrm{UB}} + 2\mathrm{h_u}d_{\mathrm{LB}} \qquad \text{Eq. 4-1}$$

$$A_{\mathrm{B}} = (s_{\mathrm{UB}} - d_{\mathrm{UB}}) \times D \qquad \text{Eq. 4-2}$$

This reduction in area will decrease the calculated capacity. However, this reduction in the loaded area is countered by the increase in the bearing area. The bearing area increases by not subtracting out the area from the u-bar to the edge of the assumed concrete triangle (h_u).

Design 2 is as follows:

$$A_{\mathrm{L}} = d_{\mathrm{UB}}D + 2\mathrm{h_u}d_{\mathrm{LB}} \qquad \text{Eq. 4-3}$$

$$A_{\mathrm{B}} = s_{\mathrm{UB}}D \qquad \text{Eq. 4-4}$$

In comparing the loaded area of Design 1 to Design 2, the loaded area is decreased which will also decrease the calculated capacity; however, the bearing area is increased in order to compensate for the loss. The bearing area now assumes the length is simply the spacing of the u-bar and does not take out the size of the u-bar as in Design 1.

Design 1 is more accurate but more complicated than Design 2. However, upon comparing the tested and calculated capacities in Table 5 according to the actual and two proposed design areas there is little discrepancy. Design 1 is only slightly more conservative and Design 2 is vastly similar to the actual values. Figure 32 gives a graphical representation of Table 5. A point above the horizontal line (the line is at

one) represents a number that is more conservative. Upon observation from Figure 32, Design 2 is sufficiently accurate and less complicated.

Table 5: Area design calculations comparison

Specimen	Graph Number	f'c	U-Bar Spacing	Joint Overlap Length	$F_{TESTED}/F_{CALCULATED}$		
		MPa	*mm*	*mm*	Acutal	Design 1	Design 2
WT-1	1	66.1	114.3	152.4	1.11	1.14	1.10
WT-2	2	53.2	114.3	152.4	1.26	1.29	1.25
WT-3	3	65.5	114.3	101.6	1.00	1.03	0.99
WT-4	4	66.0	152.4	152.4	1.07	1.12	1.09
ST-0	5	32.1	114.3	152.4	1.36	1.38	1.35
ST-7	6	68.8	114.3	152.4	1.02	1.04	1.01
FT-0	7	34.3	114.3	152.4	1.24	1.26	1.23
FT-7	8	65.5	114.3	152.4	1.15	1.18	1.14

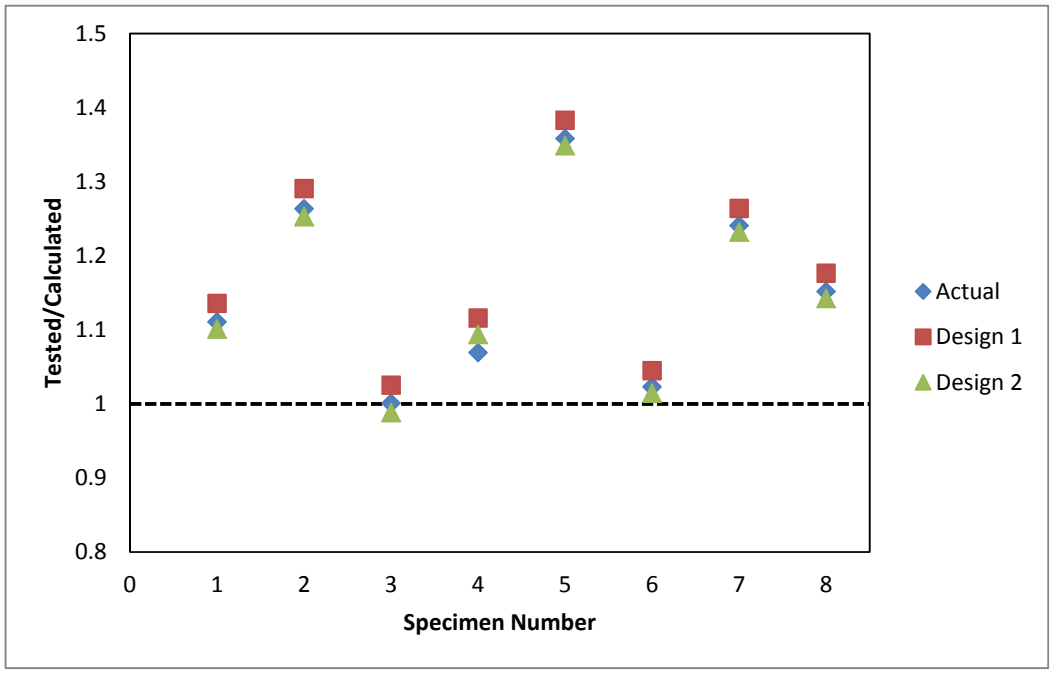

Figure 32: Comparing area design calculations

4.2 Limitations of design

The University of Tennessee have completed u-bar transverse joint tests using three different parameters: concrete compressive strength, u-bar spacing, and joint

overlap length (Chapman). Some limitations must be given to these parameters.

4.2.1 Concrete compressive strength

As the concrete compressive strengths decreased the calculated values became more conservative. Figure 14 shows that if the concrete compressive strength reaches approximately 68948 kPa (10,000 psi) then the calculated capacities mirror the tested capacities and are no longer considered conservative since the values would approximate one in Figure 14. This calculation would then not be applicable for high strength concrete and should only be used for normal weight concrete up to 68948 kPa (10,000 psi).

4.2.2 U-bar spacing

Specimen WT-4's u-bar spacing was increased to six inches from 4.5 inches resulting in an increase in ultimate capacity. This is explained in the triangular calculations due to the increase in loading and bearing areas. However, to increase the tensile capacity of the joint zone a lower u-bar spacing should be used. Table 6 represents the effect of changing the u-bar spacing and is graphically represented in Figure 33. Figure 33 which shows that as the u-bar spacing increases the triangular strength also increases. However, if the comparison is over a certain length (such as a per foot section) then the total connection's capacity is increased if a smaller spacing is used. This is due to an increase in the number of triangles formed which can be added together, as is show in Figure 34. For the 152.4 mm (6 inch) u-bar spacing there are only two triangles in the per foot section compared to six triangles for a 50.8 mm (2 inch) u-bar spacing.

Table 6: U-bar spacing capacity comparison of per triangle and per foot section

f'c	U-Bar Spacing		Joint Overlap Length	F_{TOTAL} per Linear Length	
(Mpa)	(mm)	*(in)*	*(mm)*	*(kN)*	(k)
66.1	406.4	16	152.4	374.957	84.298
66.1	355.6	14	152.4	378.443	85.082
66.1	304.8	12	152.4	385.698	86.713
66.1	254	10	152.4	398.876	89.675
66.1	203.2	8	152.4	422.18	94.91
66.1	152.4	6	152.4	465.06	104.55
66.1	101.6	4	152.4	554.42	124.64
66.1	50.8	2	152.4	811.60	182.46

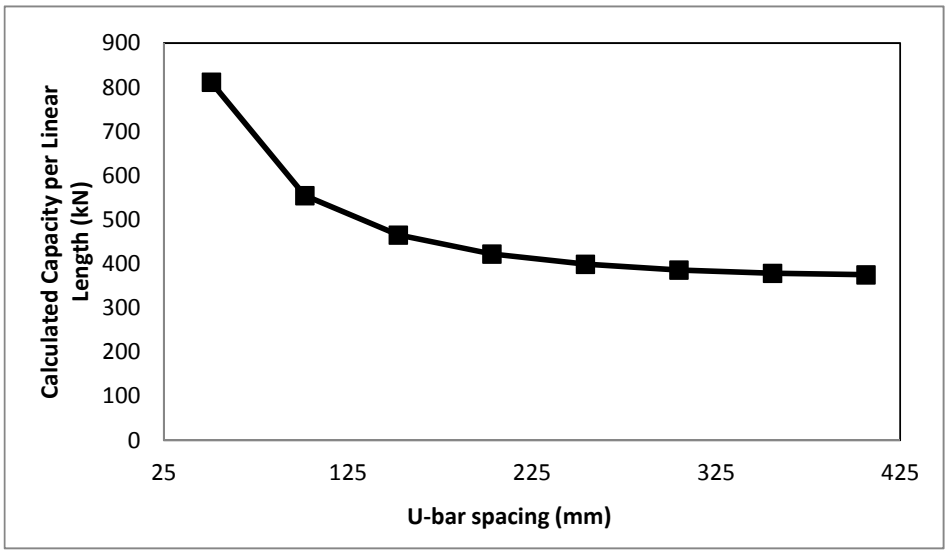

Figure 33: U-bar spacing capacity comparison

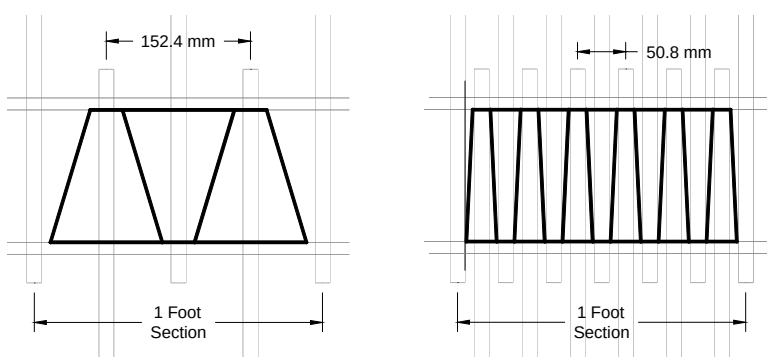

Figure 34: Comparison of the number of triangles for u-bar spacing

The minimum u-bar spacing is limited by the spacing requirements in ACI 318-08 section 7.6.1 which states that the spacing cannot be less than the diameter of the bar or 25.4 mm (one inch) (ACI 318-08). In the case of a number 5 rebar, the smallest u-bar spacing allowed by ACI 318-08 would be 82.55 mm (3.25 inches).

In terms of strength it is not logical to increase the u-bar spacing but in order to reduce costs a maximum spacing may be desired. There has been no testing done for the maximum u-bar spacing by the University of Tennessee. Eventually, however, there would be an angle which would not allow the shear capacity to develop strength once the cracks have formed. If u-bar spacing is desired to exceed six inches then it would be recommended to run further tests to determine the capacity of horizontal strengths developed once cracked.

4.2.3 Overlap length

Once the joint overlap length was reduced to 101.6 mm (4 inches) from 152.4 mm (6 inches) the capacity of the specimen was also reduced. Table 7 consist of varying joint overlap lengths with their respective capacities on a per linear length basis. Table 7 is graphically represented in Figure 35 which shows that with the increase of the joint overlap length there is an increase in the joint's strength. Therefore, with any increase of the joint overlap length there would be an increase in the joints capacity. The limitation would then come from economics since with a larger overlap length would be more concrete to pour on site. The University of Tennessee has not done testing on joint overlap lengths above 152.4 mm (6 inches). Theoretically this would increase the capacity but this would need to be verified by testing.

Chapman (2010) recommended not decreasing the joint overlap length below 152.4 mm (6 inches) since the crack widths were enlarged and inadequate ductility was experienced with an overlap length of 101.6 mm (4 inches). Chapman speculated that if a larger overlap length was desired then another lacer bar could be inserted in the middle of the joint which could provide an increase in capacity. (Chapman 2010)

Table 7: Joint overlap length capacity comparison

f'c	U-Bar Spacing	Joint Overlap Length		F_{TOTAL} per Linear Length	
(Mpa)	*(mm)*	*(mm)*	*(in)*	*(kN)*	*(k)*
66.1	114.3	50.8	2	417.70	93.91
66.1	114.3	101.6	4	469.46	105.54
66.1	114.3	152.4	6	524.57	117.93
66.1	114.3	203.2	8	583.52	131.19
66.1	114.3	254	10	644.90	144.99
66.1	114.3	304.8	12	707.81	159.13
66.1	114.3	355.6	14	771.74	173.50
66.1	114.3	406.4	16	836.38	188.04

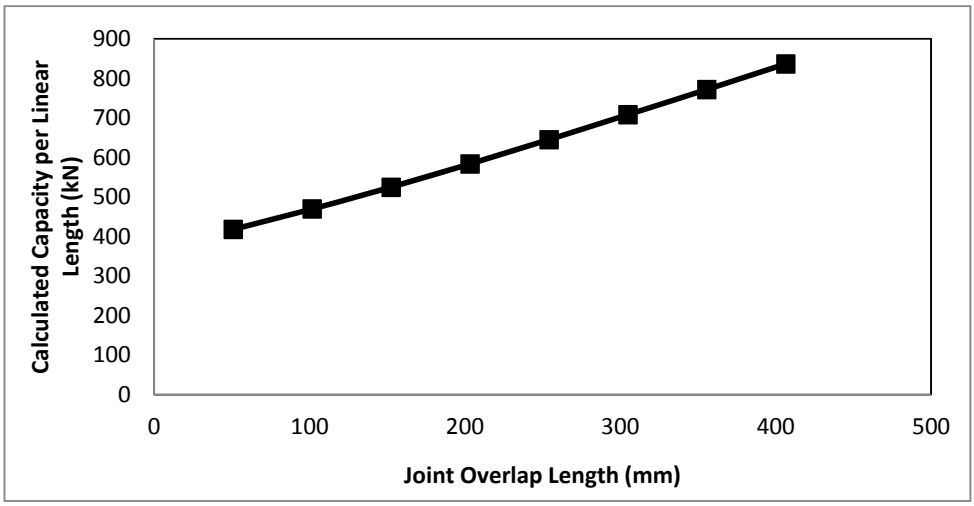

Figure 35: Joint overlap length capacity comparison

If additional design strength is required it would be recommended to decrease the u-bar spacing since the slope of the per linear length in Figure 34 is steeper for lower

u-bar spacing than the slope in Figure 35 of the change in the joint overlap length. If additional strength is required then the other options would be to increase the joint overlap length or increase the in-situ joint zone concrete compressive strength.

4.3 Lacer Bar

The lacer bar, as stated in Section 3.2, is imperative in the design given that it provides ductility, confinement, and bearing for the concrete. In order to accurately design for the lacer bar, a bending analysis must be done for the lacer bar configuration (the bending analysis has been discussed in Section 3.2). As the lacer bar deflects it causes cracking in the in-situ joint region, which is not desired for serviceability. This cracking can be decreased if the lacer bar diameter is large enough to resist the applied moment from the tensile forces. The options to consider are to increase the lacer bar size or to add additional lacer bar(s). However, the lacer bar size is limited by the required spacing between rebar according to ACI 318-08 spacing criteria which limits the size or configuration of the lacer bar(s) providing sufficient concrete flow in the joint zone. Increasing the area of the lacer bar will decrease the deflection, however, this is not a strength criteria but a serviceability requirement. In order to not over design the lacer bars or crowd the bend of the u-bar, it would be recommended to design the lacer bar with unfactored loads since this is a serviceability requirement not strength design.

In design the lacer bar needs to resist the moment applied from the loading of the u-bars and bearing of the concrete triangles. If the moment design is to remain in the elastic stage of the lacer bar then the lacer bar may exceed the spacing requirements of

ACI 318-08. Therefore, the lacer bar should be designed for the plastic moment.

From the lacer bar analysis done in section 3.2 of specimen WT-1 there is a maximum moment of 1182.9 kN-mm (10.47 k-in). First the design will be done for the elastic moment without considering reduction factors. The steel is grade 60.

$$M_y = F_y S_x \qquad \text{Eq. 4-6}$$

The section modulus for a circle is given as:

$$S_x = \frac{I}{c} = \frac{\frac{\pi \times d_b^4}{64}}{c} = \frac{\pi \times d_b^4}{64 \times {}^{d_b}/_{2}} = \frac{\pi \times d_b^3}{32}$$

Solving for the required diameter of the lacer bar and substituting the maximum moment from the analysis for the elastic moment becomes:

$$d_b = \sqrt[3]{\frac{M_u 32}{\pi F_y}} \qquad \text{Eq. 4-7}$$

$$d_b = \sqrt[3]{\frac{1182.9\ kN - mm \times 32}{\pi \times 414\ MPa}} = 30.73\ mm$$

In order to resist the moment and to keep the lacer in the elastic stage the required diameter is 30.73 mm (1.21 inches) and therefore a number 10 reinforcing bar would be required.

In order to design the lacer bar to undergo plastic bending (Equation 4-8) the plastic section modulus must be known and can be calculated by Equation 4-9:

$$M_P = F_y Z_x \qquad \text{Eq. 4-8}$$

$$Zx = \sum Ad \qquad \text{Eq. 4-8}$$

d - Distance from the centroid of the tension or compression section to the neutral axis

A - Area of the tension or compression section

For a circular cross section the plastic section modulus is given as:

$$Zx = 2 \times \left(\frac{\pi r^2}{2} \times \frac{4r}{3\pi}\right) = \frac{4r^3}{3} = \frac{{d_\mathrm{b}}^3}{6}$$

Solving for the required diameter of the lacer bar and substituting the maximum moment from the analysis for the plastic moment becomes:

$$d_\mathrm{b} = \sqrt[3]{\frac{M_\mathrm{u} 6}{F_\mathrm{y}}} \qquad \text{Eq. 4-8}$$

$$d_\mathrm{b} = \sqrt[3]{\frac{1182.9\ kN - mm \times 6}{414\ MPa}} = 25.6\ mm$$

In order to resist the moment and keep the lacer bar in the plastic stage requires a diameter of 25.6 mm (1.01 inches) and therefore a number 8 reinforcing bar could be used. If a number 8 bar is used in the same analysis done in section 2 then the maximum deflection now becomes 0.305 mm (0.012 inch) compared to a 4.52 mm (0.178 inch) maximum deflection for a number 4 bar. If only elastic deformation is allowed then the maximum deflection for a number 10 bar is 0.127 mm (0.005 inch) according to the analysis done in section 3.2.

Table 8 compares the elastic and plastic designs by giving the maximum deflections from the model with the respective number of rebar. Both maximum shear and moment values are given from the computer analysis but the moment controls what diameter would be required. The plastic design consistently requires a lower number rebar than the elastic design and deflects relatively close to the elastic design deflection.

Table 8: Comparison of elastic and plastic design

Comparison of Elastic and Plastic Design from the Computer Analysis										
Specimen	Controlling Scenario	Computer Analysis			Elastic Design			Plastic Design		
		Max Deflection (mm)	Max Shear (kN)	Max Moment (kN-m)	d_b req'd (mm^2)	# rebar	Max Deflection (mm)	d_b req'd (mm^2)	# rebar	Max Deflection (mm)
WT-1	Loading	21.29	97.90	2.25	967.9	11	0.381	811	10	0.5334
	Bearing	4.75	64.05	1.18	781.8	10	0.127	655	8	0.3048
WT-2	Loading	23.24	85.58	2.02	933.4	11	0.4064	782	9	0.9144
	Bearing	3.61	50.71	0.93	720.2	9	0.1524	603	8	0.2286
WT-3	Loading	1.75	87.49	1.53	852.2	10	0.0508	714	9	0.0762
	Bearing	16.26	71.17	1.30	805.6	10	0.4064	675	8	1.016
WT-4	Loading	21.26	108.1	2.99	1064	14	0.2032	892	11	0.381
	Bearing	21.16	83.00	1.84	905.8	11	0.254	759	9	0.8128
ST-0	Loading	24.49	54.49	1.56	857.9	10	0.3556	719	9	0.5334
	Bearing	9.73	40.09	1.12	766.5	9	0.381	643	8	0.6096
ST-7	Loading	20.85	100.4	2.29	974.5	11	0.3556	817	10	0.5334
	Bearing	2.74	67.79	1.35	817	10	0.0762	685	8	0.1778
FT-0	Loading	4.85	65.56	1.62	867.3	11	0.4318	727	9	0.9652
	Bearing	0.58	41.07	1.13	769.2	10	0.2286	645	8	0.5842
FT-7	Loading	21.39	97.37	2.24	966.6	11	0.254	810	10	0.5588
	Bearing	1.85	52.62	1.65	873.9	11	0.0254	733	9	0.0762

Even though the plastic design allows a lower number rebar to be used the rebar still remains too large for ACI 318-08 spacing criteria. The size of the aggregate must be considered to allow the concrete to flow into the radius of the u-bar which must be seventy five percent (3/4) of the minimum spacing between bars (ACI 318-08 section 3.3.2). Section 7.6.1 of ACI 318-08 specifies that the spacing of parallel bars shall be the diameter of the bar (d_b). Though the lacer bar is not parallel to the u-bar, this criterion will be applied here to further consider the flowing of concrete in this area (ACI 318-08 R7.6). Figure 36 shows the clear spacing between the u-bar and lacer bar. According to the triangular method this area is important due to the loading areas, bearing areas, and confinement within the in-situ joint zone and therefore concrete must be allowed to flow in this area. If the lacer bar diameter is

determined from the plastic design above then the clear spacing between the lacer bar and u-bar is decreased to where the spacing criteria is not met as is shown in Figure 37. The aggregate size would have to be less than 8.33 mm (0.328”) (taken from 75% of 11.11 mm (7/16”)) which would decrease the strength of the concrete. Therefore, in order to keep the spacing criteria, a limit must be placed on the size of rebar being used or a configuration of multiple lacer bars must be allowed (another option would be to increase the radius of the u-bar which would allow a larger lacer bar diameter, however, for this testing this option is not explored due to reasons specified in Chapman’s (2010) report).

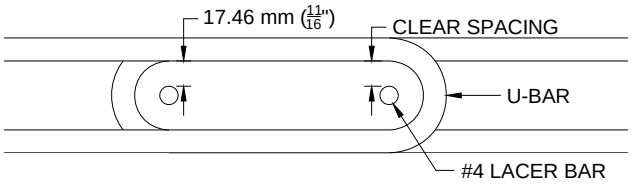

Figure 36: Clear spacing between a #4 lacer bar and u-bar

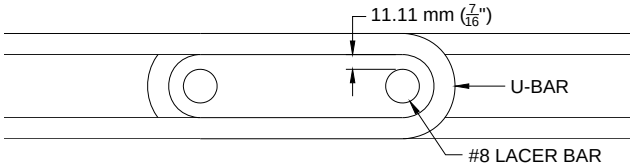

Figure 37: Clear spacing for a #8 lacer bar

If a limit is placed on the size of the lacer bars, how much would that affect the performance of the in-situ joint and what would the limit be? For a sufficient flow of concrete in the radius of the u-bar the controlling factor would be the size of the aggregate. If a number 4 is used then a half inch aggregate size could be used. If a number 5 is used then an 11.11 mm (7/16”) aggregate size could be used (75% of 15.88 mm (5/8”)). For any larger number of lacer bar the concrete may not

sufficiently flow in these areas therefore various rebar sizes are used as an example for specimen ST-0. ST-0 loading and bearing lacer bars were analyzed with different rebar sizes with their respective deflections shown in Table 9. Table 9 shows the computers modeled deflection from the corrected model discussed in section 3.2. When analyzing a number four bar the loaded side controls but when analyzing a number six bar the bearing controls. The concrete's bearing resistance explains the difference in the deflections since the bearing resistance depends on the loading or bearing condition as discussed in section 3.2. Figure 38 graphically represents Table 9 and shows that as the size of the rebar increases, there is less respective deflection decrease. For larger bars the bearing controls and in the case of a number seven bar if the concrete bearing resistance is applied as discussed in section 3.2 then the bearing resistance will cause the bar to deflect in the direction of the applied bearing resistance. The bearing resistance is meant to react to a deflection not to cause a deflection and therefore the theoretical deflection approaches but does pass (reach negative values) zero. If a rebar larger than a number seven was to be used there would be no significant decrease in deflection.

Table 9: Deflection comparison of ST-0 for different rebar sizes

Deflection of ST-0's lacer bar								
Rebar	#4		#5		#6		#7	
	(mm)	*(in)*	*(mm)*	*(in)*	*(mm)*	*(in)*	*(mm)*	*(in)*
Loaded	13.767	0.542	4.496	0.177	0.432	0.017	0.203	0.008
Bearing	9.728	0.383	3.632	0.143	1.575	0.062	0.762	0.030

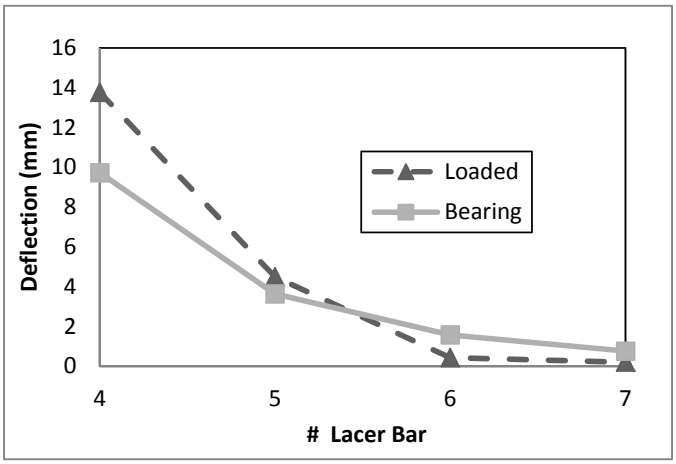

Figure 38: Deflection of ST-0 verses size of bar

Since the lacer bar should be designed for serviceability, controlled by deflection and cracking, a number eight bar would be too excessive. A number seven bar would only decrease the deflection slightly more than a number six bar. The possibility then exist that if the largest required lacer bar was a number six then the concrete being poured in the in-situ joint zone may be able to flow freely through the joint zone. According to ACI 318-08 this would reduce the aggregate size to a maximum of 10.72 mm (0.422 inch) due to the maximum of 75% of the spacing between bars in section 3.3.2 (ACI 318-08 section 3.3.2). According to the commentary (ACI 318-08 R3.3.2) these limitations may be waived by a licensed professional if "…the concrete can be placed without honeycombs or voids." (ACI 318-08 R3.3.2)

Chapter 5 Conclusion

Current decking connections produce uncontrolled flexural cracking which leads to joint leakage in the in-situ joint zone. The University of Tennessee has proposed a u-bar connection to increase flexural and tensile capacities, thereby decreasing the cracking in the joint zone. To further understand the connection, different parameters were given to the specimens as follows: concrete compressive strength, u-bar spacing, and joint overlap length. It was found that, as the u-bar spacing was increased, the capacity increased. Also, if the joint overlap length was decreased, then the capacity was decreased.

Two different methods were examined to mathematically determine the capacity of the connection. Strut and tie modeling (STM) was first examined, but if ACI's or AASHTO's STM criteria were followed the calculated capacities were significantly lower than that obtained from testing. If an increase of the strut's width was allowed, however, then the increase in capacity compared reasonably to the tested capacity.

The triangular method was proposed to determine the capacity which analyzed a triangular concrete shape. A free body diagram (FBD) of the triangular shape of the concrete in-situ joint, bounded by the u-bar and lacer bar spacing, could be analyzed and used to determine the specimen's capacity.

Both the strut and tie modeling and the triangular method produced accurate and reasonable calculated capacities compared to the tested capacities, as can be seen in Figure 39. The observed design difference was the analysis and design of the lacer bar. From testing and observation the lacer bar underwent bending deformation.

The STM method analyzed and designed the lacer bar in tension which is not correct. Even if the lacer bar was designed by STM, the resulting design produced a required #4 lacer bar. However, a #4 bar was used in testing which produced excessive bending deformation.

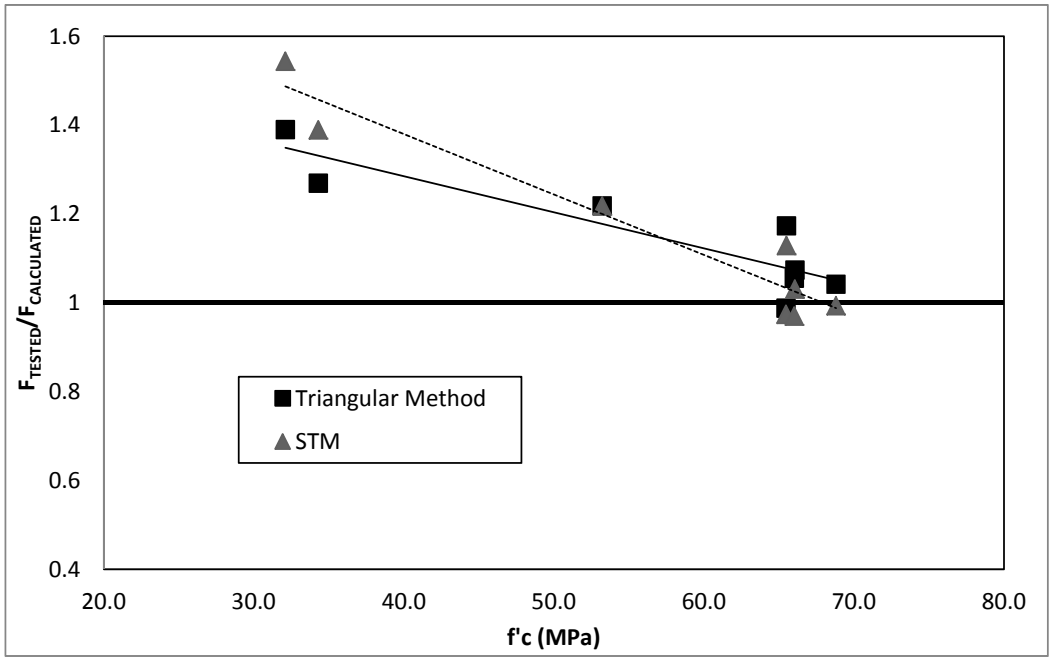

Figure 39: Comparison of the triangular method and STM calculated capacities

The triangular method allowed the lacer bar to be analyzed in bending, similar to the testing results. Parameters were given to the computer analysis which produced a similar computer analysis deflection compared to the actual measured deflection. If slight adjustments were made to the model, the computer analysis deflection resulted in the same deflection as the actual measured deflection. This analysis validated the method used and provided understanding of the function of the lacer bar in the connection joint. The adjustments made to the analysis displayed normal uncertainties in concrete shear and confinement calculations.

Moment controlled in the lacer bar design; therefore a plastic moment design is proposed to allow a simple calculation to be made. The lacer bar should be designed

for serviceability since the lacer bar assists in controlling the cracking. Also, serviceability design would prevent over-designing the lacer bars, thus allowing the concrete to flow freely around the u-bar bend.

The triangular method generates accurate capacity calculations as well as correctly modeling the connection according to the flow of forces. This method also allows the lacer bar to be analyzed and designed from the analysis.

List of References

ACI Committee 318, (2008) "Building Code Requirements for Structural Concrete (ACI 318-08) and Commentary (ACI 318R-08)," American Concrete Institute, Farmington Hills, MI.

American Association of State Highway and Transportation Officials, (2007) "AASHTO LRFD Bridge Design Specifications," Washington, D.C., 4th Edition.

Chapman, Cheryl Elizabeth, (2010) "Behavior of Precast Bridge Deck Joints with Small Bend Diameter U-Bars," (M. S.) University of Tennessee, Knoxville

Gordon, S. R.; May, I. M., (2005) "Development of In Situ Joints for Pre-Cast Bridge Deck Units," Bridge Engineering 000, Issue BEO, pp. 1-14.

Hawkins, Neil M.; Kuchma, Daniel A.; Mast, Robert F.; Marsh, M. Lee; Reineck, Karl-Heinz, (2005) "Simplified Shear Design of Structural Concrete Members," NCHRP Document 78, Appendix A

Lewis, S.; Ma, J.; French, C.E.; Burdette, E., (2009) "Longitudinal and Transverse Joint Connection Details To Achieve Precast Bridge Deck Continuity" NCHRP 10-71 Draft ACI Manuscript.

Nawy, Edward G., (2009) "Reinforced Concrete: A Fundamental Approach" 6th Edition, Prentice Hall International Series

Ong, K. C. G.; Hao J. B.; Paramasivam, P., (2006) "A Strut-and-Tie Model for Ultimate Loads of Precast Concrete Joints with Loop Connections in Tension," Construction and Building Materials 20, pp. 169-176.

Ryu, Hyung-Keun; Chang, Sung-Pil; Kim, Yong-Jin; Kim, Byung-Suk, (2005) "Crack Control of a Steel and Concrete Composite Plate Girder with Prefabricated Slabs under Hogging Moments," Engineering Structures 27, pp. 1613-1624.

Zhu, Peng, (2010) "Durability and Fatigue Behavior of CIP Concrete Connections for Accelerated Bridge Construction," (PhD dissertation) University of Tennessee, Knoxville

Vita

Richard Aaron Hanks was born in Kingsport, Tennessee, on April 26, 1985. He was raised by his parents, Richard and Glenda Hanks, in the east Tennessee area. In 2003, he graduated from Sullivan South High School in Kingsport, Tennessee. His education continued at Middle Tennessee State University until his interest in Civil Engineering surfaced after a summer trip to North Africa. During his junior year at the University of Tennessee he was accepted for the 5-year program. As a result, he began working towards his Master of Science degree during his senior year and in 2010 he received his Bachelor of Science degree in Civil Engineering from the University of Tennessee. Currently, Aaron is pursuing a Master of Science degree in Civil Engineering with a concentration in Structural Engineering at the University of Tennessee.